Nucleon-nucleon scattering from dispersion relations: Next-to-next-to-leading order study

J. A. Oller*
Departamento de Física, Universidad de Murcia, E-30071 Murcia, Spain
(Received 14 February 2014; revised manuscript received 9 September 2015; published 11 February 2016)

Nucleon-nucleon (NN) scattering is studied by applying an approach based on the N/D method and chiral perturbation theory (ChPT), whose dynamical input per partial wave consists of the imaginary part of the NN partial-wave amplitude along the left-hand cut. The latter is calculated in one-loop ChPT up to and including next-to-next-to-leading order (NNLO). A power counting for the subtraction constants is established, which is appropriate for those subtractions attached to both the left- and the right-hand cuts. A quite good reproduction of the Nijmegen partial-wave analysis phase shifts and mixing angles results, which implies a steady improvement in the accurateness achieved by increasing the chiral order in the calculation of the dynamical input. I discuss that it is not necessary to fine tune the chiral counterterms c_i determined from pion-nucleon scattering to agree with NN data, but instead one should perform the iteration of two-nucleon intermediate states in a well-defined way so as to keep proper unitarity and analyticity. It is also confirmed at NNLO the long-range correlations between the NN S-wave effective ranges and scattering lengths, when employing only once-subtracted dispersion relations, that hold up to around 10% when compared with experimental values.

DOI: 10.1103/PhysRevC.93.024002

I. INTRODUCTION

Chiral perturbation theory (ChPT) is the effective field theory of QCD at low energies [1,2]. Its paradigmatic application is the purely mesonic sector in SU(2).[1] Its extension to the one-baryon sector presents some complications owing to the large nucleon mass that does not vanish in the chiral limit [13,14], which posed interesting problems to the theory.[2] For reviews of ChPT on these topics, see, e.g., Refs. [18–23].

The extension of ChPT to systems with a larger baryonic number was considered in Ref. [24], where the chiral counting is applied to the calculation of the multinucleon potential. In these cases one also has to face the problem associated with the infrared enhancement associated with the small nucleon kinetic energies, which requires to resum the infinite string of diagrams owing to the iteration of intermediate multinucleon states. The extension of the chiral power counting to finite density system, including the contributions of multinucleon reducible diagrams, is given in Ref. [25]. For related reviews, see, e.g., Refs. [26–30].

The application of the set up of Ref. [24] to nucleon-nucleon (NN) scattering has been phenomenologically successful [31–34]. However, the sensitivity of the results on the values of the cutoff taken to solve the associated Lippmann-Schwinger equation for the iteration of two-nucleon intermediate states has given rise to a flurry of publications, whose fair and comprehensive consideration is beyond this Introduction. For more detailed accounts on this respect the reader is referred to Refs. [26,27,35–41]. The aim here is not to solve yet such a notorious problem but to offer a complementary approach based on ChPT and dispersion relations (DRs) that allows one to derive NN scattering amplitudes free of regulator dependence.

I extend here the previous work of Refs. [42–44] to study NN scattering by applying an approach based on ChPT and the N/D method of Ref. [45]. For this theory the dynamical input is not a NN potential but the discontinuities of NN partial-wave amplitudes along the left-hand cut (LHC). Namely, denoting by $T(A)$ a generic NN partial wave, with A the center of mass (c.m.) three-momentum squared, one has the LHC that extends for $A < L$, $L = -M_\pi^2/4$ with M_π the pion mass. Because of the Schwarz reflection principle, the discontinuity of $T(A)$ across the LHC fulfills that $T(A + i0^+) - T(A - i0^+) = 2i\,\Delta(A)$, where $\Delta(A)$ is the imaginary part of a NN partial-wave amplitude.

Both two-nucleon irreducible and reducible Feynman diagrams contribute to $\Delta(A)$. The former ones are amenable to a straightforward ChPT expansion in much the same way as discussed in Ref. [24] for the calculation of chiral NN potential. Remarkably, the contributions to $\Delta(A)$ stemming from two-nucleon reducible diagrams can be calculated perturbatively in the chiral expansion as well, as explained in detail in Ref. [44]. In this way, one can perform a perturbative calculation of $T(A)$ within chiral effective field theory [46] and then take its imaginary part along the LHC to determine $\Delta(A)$. Notice that short-range nuclear forces, which in a low-energy effective field theory like ChPT are accounted for by local interactions of zero range, do not contribute to $\Delta(A)$.

This approach based on the N/D method and ChPT was solved in Refs. [42,43], with $\Delta(A)$ calculated at leading order (LO) from one-pion exchange (OPE), while in Ref. [44] the NLO contributions to $\Delta(A)$ were also included from the one-loop ChPT perturbative calculation of Ref. [46]. Compared with the LO study, Ref. [44] obtained a clear improvement

*oller@um.es

[1]This even presents one corner of concern owing to the enhanced role of the right-hand cut in the isoscalar scalar pion-pion scattering [3–9], with an important impact as well in the pion-nucleon (πN) sector [10–12].

[2]A faster stabilization of the chiral series in this case has been recently accomplished [11,12,15] by combining the covariant formalism of the extended on mass shell regularization scheme (EOMS) [16] with the explicit inclusion of the $\Delta(1232)$ in the δ counting [17].

in the reproduction of the phase shifts and mixing angles of the Nijmegen partial-wave analysis (PWA) [47], referred to in the following as PWA93. I want to give one step forward here and consider the next-to-next-to-leading order (NNLO) contributions to $\Delta(A)$ from subleading two-pion exchange (TPE) [46]. A steady improvement in the reproduction of the PWA93 results when passing from NLO to NNLO, which already reproduces PWA93 accurately, so that the chiral expansion in the method used is well behaved. In addition, only convergent integrals are involved in the calculations by taking enough subtractions, and then the referred regulator dependence that typically arises when solving the Lippmann-Schwinger equation with a chiral *NN* potential is avoided by construction. An interesting outcome from the present study is that the long-range correlations between the effective range and scattering length for each of the *NN* S waves is corroborated, when only one input is taken from experiment. These correlations, first noticed in Ref. [35], were also obtained in the NLO N/D study of Ref. [44]. Note that with the approach followed here they are deduced solely from basic principles of *NN* partial-wave amplitudes, namely, chiral symmetry, unitarity, and analyticity. It is worth pointing out that one can proceed further and include more subtractions, so that one can implement within this formalism the exact values of the effective ranges unambiguously, something that is not possible, e.g., in the tighter schemes of Refs. [35,48,49].

A chiral power counting for the subtraction constants is developed below based on the running of their values under variations in the subtraction point. I show that at NLO and NNLO in the calculation of $\Delta(A)$ one then has twice-subtracted DRs. Nevertheless, on top of this criterion one has to impose (i) to end with integral equations (IEs) having meaningful solutions[3] (otherwise, the arguments driving to the power counting for the subtraction constants do not make sense because the integrals involved are not convergent) and (ii) to satisfy the proper threshold behavior for F and higher partial waves. These two requirements could imply the necessity of taking more than two subtractions in the corresponding DRs. Nevertheless, the second requirement could be softened, as explained below (Sec. III B).

It is argued in Ref. [50] that the pion-nucleon (πN) monomials proportional to the NLO counterterms c_i, produce a too-large contribution to the *NN* potential at medium and short distances when it is calculated at NNLO in dimensional regularization, which worsens the properties of the chiral expansion. Because of this, Ref. [50] advocated to employ the so-called spectral function regularization (SFR) to cut the spectral representation of the NNLO *NN* potential at around the chiral symmetry breaking scale. This last point would be equivalent to truncating the full extent of the LHC in the dispersive integrals, as also remarked in Ref. [51]. However, I would like to stress that this is not necessary to obtain a good reproduction of PWA93 when employing $\Delta(A)$ determined up to NNLO in the method used in this work. The definitive improvement of the results here does not arise by modifying the two-nucleon irreducible diagrams at NNLO, but by performing the iteration of two-nucleon unitarity diagrams in a proper way, such that the right analytical properties of a *NN* partial wave are not distorted.

The N/D technique, in conjunction with ChPT, was also applied recently to study *NN* partial-wave amplitudes in Ref. [51], following the ideas employed in other works [52–56]. This approach is based on a nonlinear IE for the partial-wave amplitudes along the right-hand cut (RHC), which results from a partial-wave DR in which there is an explicit separation between the RHC and LHC contributions. Here all the contributions from the LHC are collected in the so-called generalized potential $U(s)$. In each channel Ref. [51] solves the nonlinear IE numerically using the N/D techniques, with $\Delta(A)$ calculated from covariant ChPT up to NNLO.[4] However, the contributions in $\Delta(A)$ for $A < -9M_\pi^2/4$ in the LHC are truncated, because it is considered that they cannot be accurately calculated in ChPT. They are then mimicked as short-range interactions so that their contributions to $U(s)$ are calculated in the physical region by means of a conformal mapping, which also extends $U(s)$ smoothly to a constant for energies above the two-pion production threshold.

An important point in the approach of Ref. [51] is that the resulting partial wave is assumed to be perturbative at the subthreshold c.m. energy μ_M, the so-called matching point, so that it is by construction the same as the one calculated perturbatively in covariant ChPT. In this way the number of coefficients of the Taylor expansion in the conformal variable is chosen to be the same as the number of ChPT counterterms at each chiral order and are fitted to *NN* phase shifts partial wave by partial wave. Phenomenologically, the phase shifts obtained in Ref. [51] for the lower *NN* partial waves reproduce data in reasonable good agreement. The residual scale dependence of the results in μ_M and Λ_s (the latter enters in the conformal mapping applied) is studied in detail in Ref. [51].

The N/D method is a powerful tool to study two-body scattering in the limit case of neglecting the LHC contributions. This is based on the fact that the general form of the solutions to the N/D IEs when $\Delta(A) \to 0$ can be given algebraically, as deduced in Ref. [4]. This solution was afterwards fixed by matching with chiral effective field theory for S- and P-wave meson-meson scattering with great phenomenological success. However, in *NN* scattering the LHC contributions are not typically perturbative because OPE can be particularly strong in some triplet partial waves [25,36,57]. Nonetheless, this fact could be tempered by increasing the number of subtractions.

After this Introduction I review the approach based on the N/D method [45] for coupled and uncoupled partial waves in Sec. II. The function $\Delta(A)$ is discussed in Sec. III, where I also elaborate the chiral power counting for the subtraction

[3]By a meaningful solution I mean here a mathematical solution to the IE that does not depend on the the number of points employed and the arbitrary large extension of the LHC on which they lie when performing the numerical discretization to solve the IE.

[4]The fulfillment of the nonlinear IE guarantees that the solutions obtained in Ref. [49] are free of ghost states, so that they have the right analytical properties. The solutions obtained within the approach followed here do not present either ghost states.

constants. Sections IV to XIII are devoted to discussing the results obtained for the different NN partial waves up to $J = 4$ (some aspects of the uncoupled waves $^1H_5$ and $^3H_5$ are also discussed). There it is shown that a quite good reproduction of the PWA93 phase shifts and mixing angles results [47], including also in the figures for comparison the results from the potentials Nijm2, Reid93 [58], AV18 [59], and the recent PWA [60]. In these sections I also compare with the one-loop ChPT perturbative approximation for higher partial waves and discuss on the relative importance of the different contributions to $\Delta(A)$. The concluding remarks are given in Sec. XIV. Finally, I discuss in the Appendix a novel and efficient numerical method to calculate higher-order shape parameters of the NN S waves.

II. DEVELOPMENT OF THE FORMALISM BASED ON THE N/D METHOD

A detailed presentation of my approach based on the N/D method [45] can be found in Ref. [44]. Here I only reproduce the main facets of the formalism.

A. Uncoupled partial waves

An uncoupled NN partial wave is written as the quotient of two functions,

$$T(A) = \frac{N(A)}{D(A)}. \tag{1}$$

In the following I use the spectroscopic notation and denote by $^{2S+1}L_J$ the different NN partial waves with S the total spin, L the orbital angular momentum, and J the total angular momentum. The reason to split $T(A)$ in two functions is because as a result of it $N(A)$ has only LHC while $D(A)$ has only RHC or unitarity cut. The following expressions for the discontinuities of the functions $N(A)$ and $D(A)$ along their respective cuts then arise:

$$\begin{aligned} \mathrm{Im}D(A) &= -\rho(A)N(A), \quad A > 0, \\ \mathrm{Im}N(A) &= \Delta(A)D(A), \quad A < L. \end{aligned} \tag{2}$$

Here $\rho(A)$ is the phase-space factor

$$\rho(A) = \frac{m\sqrt{A}}{4\pi}, \tag{3}$$

where m is the nucleon mass. The first of the relations in Eq. (2) is a consequence of elastic unitarity, while the last one stems from the definition of $\Delta(A)$ given above.

Standard DRs for the functions $D(A)$ and $N(A)$ are derived in Ref. [44] under the assumption that the function $D(A)$ does not diverge faster than a polynomial of degree n_0 for $A \to \infty$. Then for $n > n_0$ one can write [44]

$$\begin{aligned} D(A) &= \sum_{i=1}^{n} \delta_i (A-C)^{i-1} - \frac{(A-C)^n}{\pi} \\ &\times \int_0^\infty dq^2 \frac{\rho(q^2)N(q^2)}{(q^2-A)(q^2-C)^n}, \end{aligned}$$

$$\begin{aligned} N(A) &= \sum_{i=1}^{n} \nu_i (A-C)^{i-1} + \frac{(A-C)^n}{\pi} \\ &\times \int_{-\infty}^{L} dk^2 \frac{\Delta(k^2)D(k^2)}{(k^2-A)(k^2-C)^n}, \end{aligned} \tag{4}$$

where C is the subtraction point. In addition, it is clear from Eq. (4) and the standard theory of DRs [61] that different values for the subtraction points can be taken in each function separately. Indeed, for many partial waves I take the subtractions for the function $D(A)$ in two points, one at $C = 0$ and the other at $C = -M_\pi^2$. This is motivated by the fact that one can always choose the normalization

$$D(0) = 1 \tag{5}$$

by dividing simultaneously $D(A)$ and $N(A)$ by a constant, an operation that obviously leaves invariant $T(A)$ [Eq. (1)]. In this way, one subtraction for $D(A)$ is always taken at $C = 0$ to guarantee straightforwardly the normalization Eq. (5).[5] Note also that the well-known uncertainty in the solution of the N/D method [45], owing to the possible presence of Castillejo-Dalitz-Dyson poles [62] in the $D(A)$ function, can be traded to a subtractive polynomial. This can be achieved by multiplying simultaneously the original functions $D(A)$ and $N(A)$ by a polynomial [which leaves $T(A)$ invariant], whose roots contain all the poles of the additive rational function in $D(A)$.[6]

To solve $D(A)$ one substitutes the expression for $N(A)$ into the DR of $D(A)$ in Eq. (4). A linear IE for $D(A)$ is then obtained:

$$\begin{aligned} D(A) &= \sum_{i=1}^{n} \delta_i (A-C)^{n-i} - \sum_{i=1}^{n} \nu_i \frac{(A-C)^n}{\pi} \\ &\times \int_0^\infty dq^2 \frac{\rho(q^2)}{(q^2-A)(q^2-C)^{n-i+1}} \\ &+ \frac{(A-C)^n}{\pi^2} \int_{-\infty}^{L} dk^2 \frac{\Delta(k^2)D(k^2)}{(k^2-C)^n} \\ &\times \int_0^\infty dq^2 \frac{\rho(q^2)}{(q^2-A)(q^2-k^2)}. \end{aligned} \tag{6}$$

Notice that the same number of subtractions for both $D(A)$ and $N(A)$ are taken in Eq. (4), which guarantees that the integrals along the RHC present in Eq. (6) are convergent [a fact that would be spoiled if the number of subtractions in $N(A)$ were larger than in $D(A)$]. The key point of the method is to solve numerically the linear IE of Eq. (6), which provides the knowledge of $D(A)$ for $A < L$. Once $D(A)$ is known along the LHC, one can calculate all the functions $D(A)$, $N(A)$, and $T(A)$ in the whole A-complex plane. To obtain $D(A)$, one can

[5] The normalization condition is real so that the function $D(A)$ always fulfills the Schwarz reflection principle.

[6] Poles with complex pole positions appear always in complex conjugate pairs because one can always make that the Schwarz reflection principle is fulfilled by the functions $D(A)$ and $N(A)$. This implies a real polynomial on the A-real axis which does not spoil unitarity.

use Eq. (6) and for $N(A)$ the second of the DRs in Eq. (4) is adequate.

The integrations along the RHC in Eq. (6) can be done algebraically in terms of the function

$$g(A,k^2) \equiv \frac{1}{\pi}\int_0^\infty dq^2 \frac{\rho(q^2)}{(q^2-A)(q^2-k^2)} = \frac{im/4\pi}{\sqrt{A+i0^+}+\sqrt{k^2+i0^+}}. \quad (7)$$

The $+i0$ is necessary for negative A or k^2, with the prescription $\sqrt{-1\pm i0} = \pm i\pi$. One can calculate the other RHC integrals of Eq. (6) with higher powers of the factor (q^2-C) in the denominator by simple differentiation of $g(A,k^2)$ with respect to C.

B. Coupled partial waves

For the case of the triplet partial waves with total angular momentum J one has the mixing between the partial waves with $\ell_1 = J-1$ and $\ell_2 = J+1$, except for the $^3P_0$. In this case I denote the different coupled partial waves by $t_{ij}(A)$, $i,j = 1,2$, which are gathered in the 2×2 matrix $T(A)$. The relation with the S matrix in my notation is

$$S(A) = I + 2i\rho(A)T(A) = \begin{pmatrix} \cos 2\varepsilon_J\, e^{2i\delta_1} & i\sin 2\varepsilon_J\, e^{i(\delta_1+\delta_2)} \\ i\sin 2\varepsilon_J\, e^{i(\delta_1+\delta_2)} & \cos 2\varepsilon_J\, e^{2i\delta_2} \end{pmatrix}, \quad (8)$$

where I is the unit matrix, ε_J is the mixing angle, and δ_1 and δ_2 are the phase shifts. Equation (8) corresponds to the Stapp parametrization [63]. Now the N/D approach explained for the uncoupled waves in Sec. II A is extended to the coupled channel case [43,44] by writing down three N/D equations, one for every $t_{ij}(A)$ [notice that because of time reversal $t_{12}(A) = t_{21}(A)$]. The main difference with respect to the uncoupled case is that now the discontinuity along the RHC of the inverse of $t_{ij}(A)$ does not simply correspond to $-\rho(A)$, but it also contains information on the other coupled partial waves. In the following I employ the notation

$$\mathrm{Im}\frac{1}{t_{ij}(A)} \equiv -\nu_{ij}(A), \quad A>0. \quad (9)$$

From Eq. (8) it is straightforward to obtain the following expressions for the $\nu_{ij}(A)$ [43,44],

$$\nu_{ii}(A) = \rho(A)\left[1-\frac{\frac{1}{2}\sin^2 2\varepsilon_J}{1-\cos 2\varepsilon_J\cos 2\delta_i}\right]^{-1},$$
$$\nu_{12}(A) = 2\rho(A)\frac{\sin(\delta_1+\delta_2)}{\sin 2\varepsilon_J}. \quad (10)$$

In terms of them one has analogous DRs as in Eq. (4), but now distinguishing between the different $D_{ij}(A)$ and $N_{ij}(A)$, $t_{ij}(A) = N_{ij}(A)/D_{ij}(A)$, and employing $\nu_{ij}(A)$ instead of simply $\rho(A)$ [44]. The subtractions constants for $D_{ij}(A)$ and $N_{ij}(A)$ are indicated by $\delta_p^{(ij)}$ and $\nu_p^{(ij)}$, respectively. Note that $\delta_1^{ij} = 1$ because of the normalization condition of Eq. (5).

Because the functions $\nu_{ij}(A)$ depend on the phase shifts δ_1, δ_2 and the mixing angle ε_J, which also constitute the final output of the calculation, I follow an iterative approach [43]. Given an input for δ_1, δ_2, and ε_J, one solves the three IEs for $D_{ij}(A)$ along the LHC so that the scattering amplitudes on the RHC can be calculated. In terms of them, the phase shifts δ_1 and δ_2 are obtained from the phase of the S-matrix elements S_{11} and S_{22}, while $\sin 2\varepsilon_J = 2\rho|t_{12}|N_{12}/|N_{12}|$, according to Eq. (8). In this way a new input set of ν_{ij} functions is provided. These are used again in the IEs, and the iterative procedure is finished when convergence is found [typically, the difference between two consecutive iterations in the three independent functions $D_{ij}(A)$ along the LHC is required to be less than one per thousand].

C. Higher partial waves

An uncoupled NN partial wave with $\ell \geqslant 1$ should vanish at threshold as A^ℓ. One has the analogous result for a coupled partial wave but in terms of $\ell_{ij} \equiv (\ell_i+\ell_j)/2$, with $i,j = 1,2$. As discussed in Ref. [44] this threshold behavior is enforced by taking at least ℓ or ℓ_{ij} subtractions at $C=0$ in the DR for $N(A)$ or $N_{ij}(A)$, respectively, and setting $\nu_p = 0$ ($\nu_p^{(ij)} = 0$) for $p = 1,\ldots,\ell$ (ℓ_{ij}). In this way, one ends with the following DRs:

uncoupled case

$$D(A) = 1 + \sum_{p=2}^{\ell}\delta_p A^{p-1} + \frac{A^\ell}{\pi}\int_{-\infty}^{L} dk^2 \frac{\Delta(k^2)D(k^2)}{(k^2)^\ell} g(A,k^2), \quad (11)$$

$$N(A) = \frac{A^\ell}{\pi}\int_{-\infty}^{\ell} dk^2 \frac{\Delta(k^2)D(k^2)}{(k^2)^\ell(k^2-A)}, \quad (12)$$

$$\delta_p = \frac{1}{(p-1)!}D^{(p-1)}(0), \quad p = 2,3,\ldots, \quad (13)$$

coupled case

$$D_{ij}(A) = 1 + \sum_{p=2}^{\ell_{ij}}\delta_p^{(ij)} A(A-C)^{p-2} + \frac{A(A-C)^{\ell_{ij}-1}}{\pi} \times \int_{-\infty}^{L} dk^2 \frac{\Delta_{ij}(k^2)D_{ij}(k^2)}{(k^2)^{\ell_{ij}}} g_{ij}(A,k^2,C;\ell_{ij-1}), \quad (14)$$

$$N_{ij}(A) = \frac{A^{\ell_{ij}}}{\pi}\int_{-\infty}^{L} dk^2 \frac{\Delta_{ij}(k^2)D_{ij}(k^2)}{(k^2)^{\ell_{ij}}(k^2-A)}, \quad (15)$$

$$\delta_p^{(ij)} = \frac{(-1)^p}{C^{p-1}}\left[\sum_{n=0}^{p-2}\frac{(-1)^n}{n!}C^n D_{ij}^{(n)}(C) - 1\right], \quad p = 2,3,\ldots, \quad (16)$$

where the derivative of order n of $D(A)$ is denoted by $D^{(n)}(A)$ and the function $g_{ij}(A,k^2,C;m)$ is defined as [44]

$$g_{ij}(A,k^2,C;m) = \frac{1}{\pi}\int_0^\infty dq^2 \frac{\nu_{ij}(q^2)(q^2)^m}{(q^2-A)(q^2-k^2)(q^2-C)^m}, \quad (17)$$

which can be expressed algebraically as a combination of $g(x,y)$'s [Eq. (7)] with different arguments. Although in this way there is a proliferation of subtraction constants (which are

not constrained) in the function $D(A)$ as ℓ (ℓ_{ij}) grows, most of them play a negligible role. This is so because NN partial waves with ℓ or ℓ_{ij} greater than 2 are quite perturbative [44,46]. In practical terms it is found found at NNLO, as well as at NLO [44], that for higher partial waves only δ_ℓ (or $\delta^{(ij)}_{\ell_{ij}}$), if any, is needed to fit data, with the rest of them fixed to zero. Furthermore, no significant improvement in the reproduction of data or in the fitted values is observed by releasing δ_i or $\delta^{(ij)}_i$, with $1 < i < \ell$ or ℓ_{ij}, respectively, so that the fit is stable. This is called in Ref. [44] the *principle of maximal smoothness* (reasons for this name are given in the same reference). In some cases, it happens that δ_ℓ or $\delta^{(ij)}_{\ell_{ij}}$ is also zero and then one says that for this partial wave the subtraction constants have *pure perturbative values*. The principle of maximal smoothness, at the practical level, is not in contradiction with the fact that the subtraction constants change their values depending on the subtraction point. The reason is that for higher partial waves at low energies the resulting $D(A)$ is close to 1 and rather smooth, its departure from this value being governed mostly by the subtraction constant multiplying the largest power of A. The latter is fixed by the degree of the subtractive polynomial and then the value of the accompanying subtraction constant is nearly independent of the precise value taken for the subtraction under changes in its value of $\mathcal{O}(M_\pi)$.

I further study in this work the perturbative character of NN partial waves with ℓ (ℓ_{ij}) $\geqslant 2$ by comparing the full outcome from the N/D equations with the result corresponding to the perturbative one-loop calculation in ChPT of Ref. [46]. In this case there is no dependence on any of the subtraction constants δ_p or $\delta^{(ij)}_p$ and, indeed, I show below that the results are typically rather similar to the full ones for $\ell_{ij} \geqslant 3$, although the latter reproduce closer PWA93, as one should expect.

III. THE INPUT FUNCTION $\Delta(A)$

In the present work $\Delta(A)$ is taken from the one-loop calculation of Ref. [46] in ChPT, which allows us to include all the contributions in $\Delta(A)$ up to $\mathcal{O}(p^3)$ or NNLO, in the counting settled in Ref. [44], which comprise OPE plus leading and subleading TPE.[7] At this order, for a given partial wave, $\Delta(A)$ diverges at most as $\lambda(-A)^{3/2}$ for $A \to -\infty$, with λ a constant. As discussed in Ref. [44], when $\lambda < 0$ one can have solutions for the IE providing $D(A)$ in the once-subtracted case, even with a divergent $\Delta(A)$ for $A \to -\infty$. However, λ is not always negative, as shown below, and then more subtractions are required to end with a meaningful IE.

[7]The covariant calculation of the once-iterated OPE contribution is performed in Refs. [64,65], which explicitly shows that the $1/m$ expansion does not converge at $\mathbf{q}^2 = -4M_\pi^2$, with $\mathbf{q}^2$ the squared of the momentum transferred. This is also the case for some other two-nucleon irreducible diagrams [65]. Nevertheless, one should stress that this pathological behavior is restricted to just a very narrow interval around the TPE branch point at the LHC. Furthermore, the calculation of Ref. [46] is standard in any potential approach on NN scattering [64]; see, e.g., Refs. [32–34,38,39], the recent reviews [26–30], and references therein. Certainly it would be of interest to apply a relativistic version of the method followed here and use a covariant calculation of $\Delta(A)$. Recent covariant studies of NN dynamics can be found in Refs. [51,64–66].

TABLE I. Different sets of values for the $\mathcal{O}(p^2)$ πN LECs c_1, c_3, and c_4.

Analysis	c_1 (GeV^{-1})	c_3 (GeV^{-1})	c_4 (GeV^{-1})
GW-HBChPT [69]	-1.13	-5.51	3.71
KH-HBChPT [69]	-0.75	-4.77	3.34
GW-EOMS [11]	-1.50 ± 0.007	-6.63 ± 0.31	3.68 ± 0.14
KH-EOMS [11]	-1.26 ± 0.14	-6.74 ± 0.38	3.74 ± 0.16
GW-IR [70]	-1.32 ± 14	-6.9 ± 6	3.66 ± 0.33
KH-IR [70]	-1.08 ± 0.15	-7.0 ± 0.7	3.72 ± 0.32
NN study [71]	-0.76 ± 0.7	-4.78 ± 0.10	3.96 ± 0.22
GW-UChPT [11]	-1.11 ± 0.02	-4.78 ± 0.04	3.04 ± 0.02
KH-UChPT [11]	-1.04 ± 0.02	-4.48 ± 0.05	3.00 ± 0.02
KH [72]	-0.81 ± 0.12	-4.70 ± 1.16	3.40 ± 0.04

A. NLO πN counterterms

At NNLO the function $\Delta(A)$ is sensitive to the NLO πN ChPT low-energy constants (LECs) c_1, c_3, and c_4. Their values are taken from different works in the literature, which are summarized in Table I. Within the same reference I distinguish, when appropriate, between those values obtained by fitting phase shifts from the Karlsruhe-Helsinki group (KH) [67] or the George Washington University group (GW) [68].

Reference [69] performs an $\mathcal{O}(p^4)$ heavy-baryon ChPT (HBChPT) study of πN scattering data. I take its values instead of the ones from the older HBChPT studies at $\mathcal{O}(p^3)$ and $\mathcal{O}(p^4)$ [73]. I include too the values from Lorentz covariant ChPT obtained in Ref. [11] by fitting πN phase shifts making use of EOMS at $\mathcal{O}(p^3)$. Furthermore, I show in the table the c_i's obtained in the covariant $\mathcal{O}(p^3)$ ChPT study of Ref. [70] employing infrared regularization (IR). However, owing to the better convergence of the πN scattering amplitude in EOMS than in IR [11,12] I give results only for the values obtained within EOMS [11]. The resulting uncertainty band is already wide enough to take into account further uncertainties that would result by considering explicitly the c_i's from the IR study of Ref. [70], which indeed are rather close to those obtained in EOMS [11]. The values from Ref. [71], obtained in a NN scattering study, are very similar to those of KH-HBChPT [69], so that in the following the former are not considered. Again the uncertainty estimated takes into account the variation in the results that would stem from the use of the the c_i's from Ref. [71]. I also give the resulting values from the fits to πN data within unitarized EOMS ChPT obtained in Ref. [11]. These are the fits that provide more stable values under the change of data between KH and GW. These values are rather similar to those from the set KH-HBChPT [69]. The values for the c_i from the work [72] are shown in the last row. This set is well covered by the values already discussed and are not considered any further. In summary, when discussing results I take into account the values for the LECs c_i obtained in Refs. [69] and [11], namely, rows 2, 3, 4, 5, 9, and 10 in Table I.

B. Number of subtractions in the chiral expansion of $\Delta(A)$

An interesting point to discuss is the appropriate number of subtractions for a given chiral order in the calculation of $\Delta(A)$ by establishing a low-energy chiral power counting for the subtraction constants. This can be accomplished by considering the running of the subtraction constants under variations of the subtraction point in the low-energy region. Let us consider first the chiral order for the subtraction constants appearing in $N(A)$. For definiteness, let us employ a twice-subtracted DR,

$$N(A) = \nu_1 + \nu_2 A + \frac{A^2}{\pi}\int_{-\infty}^{L} dk^2 \frac{\Delta(k^2)D(k^2)}{(k^2)^2(k^2-A)}. \tag{18}$$

Now let us move the subtraction point from zero to $C = \mathcal{O}(M_\pi^2)$. It is then straightforward to show that the previous DR can be rewritten as[8]

$$\begin{aligned} N(A) &= \nu_1' + \nu_2' A + \frac{(A-C)^2}{\pi}\int_{-\infty}^{L} dk^2 \frac{\Delta(k^2)D(k^2)}{(k^2-C)^2(k^2-A)}, \\ \nu_1' &= \nu_1 - \frac{C^2}{\pi}\int_{-\infty}^{L} dk^2 \frac{\Delta(k^2)D(k^2)}{(k^2-C)^2 k^2}, \\ \nu_2' &= \nu_2 + \frac{C}{\pi}\int_{-\infty}^{L} dk^2 \frac{\Delta(k^2)D(k^2)}{(k^2-C)^2 k^2}\frac{2k^2-C}{k^2}. \end{aligned} \tag{19}$$

Here one takes $C = \mathcal{O}(p^2)$; k^2 can also be counted as $\mathcal{O}(p^2)$, because the result of a convergent integral at low energies is dominated by the low-energy region of the integrand, while the function $D(k^2)$ is counted as $\mathcal{O}(p^0)$ because $D(0) = 1$. Furthermore, because at LO $\Delta(k^2) = \mathcal{O}(p^0)$, it follows from Eq. (19) that $\nu_1 = \mathcal{O}(p^0)$ and $\nu_2 = \mathcal{O}(p^{-2})$. This procedure can be easily generalized so that $\nu_n = \mathcal{O}(p^{-2(n-1)})$. By increasing the chiral order in the calculation of $\Delta(A)$ up to $\mathcal{O}(p^m)$ the ν_n will receive an extra contribution starting at $\mathcal{O}(p^{-2(n-1)+m})$, as it is also clear from Eq. (19). Now the point is to demand that

$$-2(n-1) + m \geqslant 0, \tag{20}$$

so that the chiral dimension for a given subtraction constant is positive or zero, because short-distance physics gives rise to contributions that do not vanish in the chiral limit.[9] Then the raising in the chiral dimension of ν_n with m until the nominal one, Eq. (20), must come from powers of M_π, $|C|^{\frac{1}{2}} \sim M_\pi$.[10] The condition in Eq. (20) determines the appropriate number of subtraction constants for a given chiral order in the calculation of $\Delta(A)$.

It is also worth noticing that ν_n is multiplied by $(A-C)^{n-1}$, so that the chiral order of $\nu_n(A-C)^{n-1}$ is always m for any n, which corresponds to the chiral order of the dispersive integral with the $\mathcal{O}(p^m)$ contribution of $\Delta(A)$. This power counting coincides with the standard Weinberg chiral power counting [24] for short-range operators, which is based on naive dimensional analysis, and that is applied to the calculation of the NN potential. For alternative suggestions on the power counting of NN counterterms, see Refs. [36,37,40,74].

One can proceed analogously for the function $D(A)$. I also exemplify it by writing down a twice-subtracted DR for $D(A)$,

$$D(A) = 1 + \delta_2 A - \frac{A(A-C)}{\pi}\int_0^\infty dq^2 \frac{\rho(q^2)N(q^2)}{q^2(q^2-C)(q^2-A)}. \tag{21}$$

Let us change the subtraction point from C to E. Because the normalization $D(0) = 1$ is fixed, the position of the first subtraction taken at $A = 0$ is not changed. As a result of this rewriting one obtains the evolution

$$\delta_2 \to \delta_2 + \frac{C-E}{\pi}\int_0^\infty dq^2 \frac{\rho(q^2)N(q^2)}{q^2(q^2-E)(q^2-C)}. \tag{22}$$

For ascribing the chiral order to δ_n, $n \geqslant 2$, one has, as before, that $C \sim E \sim M_\pi^2$, $q^2 = \mathcal{O}(p^2)$. Importantly, the phase-space factor that appears in the integrals along the RHC is counted as

$$\rho(q^2) = \mathcal{O}(p^0) \tag{23}$$

because it involves the product $m\sqrt{q^2}$ and $m/M_\pi \gg 1$. One then concludes from Eqs. (22) and (23) that $\delta_2 = \mathcal{O}(p^{-2})$ for the LO contribution of $N(A) = \mathcal{O}(p^0)$. This result can be generalized easily to more subtractions so that $\delta_n = \mathcal{O}(p^{-2(n-1)})$. However, this chiral order increases when considering higher-order contributions to $N(A)$, stemming from higher orders in the calculation of $\Delta(A)$, which give rise to contributions of the same order in $N(A)$. Thus, once they are taken into account, there is the corresponding rise in the chiral order of δ_n, so that now $\delta_n = \mathcal{O}(p^{-2(n-1)+m})$ and the chiral orders of ν_n and δ_n are the same. Indeed, this is a necessary result because, according to the general formalism of Sec. II, the same number of subtractions are taken in both $D(A)$ and $N(A)$. The fulfillment of this requirement is also another reason for taking $\rho = \mathcal{O}(p^0)$ in the chiral counting. It is worth stressing that the chiral power counting for the subtraction constants δ_n corresponds to two-nucleon reducible diagrams,[11] while the standard Weinberg chiral power counting for nuclear interactions [24] only involves two-nucleon irreducible diagrams.

Note also that Eqs. (19) and (22) show in a simple and explicit way how the subtraction constants evolve when changing the subtraction point. In contrast, it is not possible, in the general case, to know *a priori* the evolution

[8] For that one can rewrite the factor $A^2/(k^2)^2$ in the integral of Eq. (18) as $([A-C]+C)^2/(k^2-C)^2 \times (k^2-C)^2/(k^2)^2$ and then isolate the factor $(A-C)^2/(k^2-C)^2$. The rest of terms can be reabsorbed in the polynomial on the right-hand side (r.h.s.) of Eq. (18).

[9] As a result, they are counted as $\mathcal{O}(p^0)$.

[10] One could ask about the fact that the chiral dimension for the other contributions to $\Delta(A)$ of order $m' < m$ could imply a negative $-2(n-1)+m'$ with $n \leqslant n_0$. This already occurs, e.g., in the paradigmatic example of ChPT, namely, meson-meson scattering. The point is to realize that these extra long-range physics contributions cancel explicitly with other contributions stemming from the rearrangement of the dispersive integral, which was done already with less subtractions when including only lower orders in $\Delta(A)$.

[11] This is apparent from the factor $q^2 - A$ in the denominator of the RHC integral in Eq. (21).

of chiral counterterms to absorb cutoff dependence when solving a Lippmann-Schwinger equation [37,75], though it could be computed numerically afterwards to require cutoff independence in the results [35,36,48,49]. Nonetheless, the limit cutoff $\to \infty$ does not always exists for the renormalized physical magnitudes [48,49]. In configuration space by making use of energy-independent short-distance boundary conditions in the Schrödinger equation one can deduce general algebraic rules on the behavior of renormalized phase shifts when the radial cutoff tends to zero for both regular and singular potentials [48].

Although the arguments offered here correspond to the uncoupled case, the same results follow for the coupled-channel partial waves because the function $\nu_{ij}(A)$ [Eq. (9)] shares the same chiral counting as $\rho(A)$, because the T matrix is $\mathcal{O}(p^0)$.[12] In summary, for $\Delta(A)$ calculated up to $\mathcal{O}(p^m)$ one has the following power counting for the subtraction constants:

$$\nu_n, \delta_n \sim \mathcal{O}(p^{-2(n-1)+m}). \tag{24}$$

Now by applying the requirement that $-2(n-1)+m \geqslant 0$ it results that in the present study at NNLO one should properly take two subtractions ($n = 2$) because $m = 3$.

Before applying Eq. (24) to a NN partial wave one has to take into account two points:

(1) For Eq. (24) to make sense one really needs that the resulting IE has well-defined solutions; otherwise, the chiral counting for the subtraction constants does not even make sense, because the integrals in Eqs. (19) and (22) would be divergent in the high-energy region. If this is the case, more subtractions have to be taken than expected from Eq. (24) until the IE becomes well-defined (with convergent DR integrals). This possible mismatch reflects a deep point: The ultraviolet region in the DR integrals is the one that controls whether an IE is convergent or not (this was analyzed in detail in Ref. [44]), while the chiral power counting reflects the infrared region (the one controlled by the chiral EFT).

(2) The exact threshold behavior of a partial wave (cf. Sec. II C) is satisfied in this work. Certainly, one could also try to soften this criterion and consider that the violation of the threshold behavior in higher partial waves is attributable to imperfections in the input function which should be tempered when increasing the order in the calculation of $\Delta(A)$. However, this is not explored in this work because, I think, it is physically more feasible to keep the exact threshold behavior. Otherwise, higher partial waves could generate too large contributions to physical observables, which are certainly suppressed at low energies because of the aforementioned threshold behavior. Then, as discussed in Sec. II C, one takes $\ell \geqslant 3$ ($\ell_{ij} \geqslant 3$) subtractions for F and higher partial waves. In addition, at the practical level the principle of maximal smoothness is invoked, so that only one or none free parameter remains.

[12]With $\rho = \mathcal{O}(p^0)$ it is also true that $\mathrm{Im}t_{ij} = \mathcal{O}(p^0)$; because of unitarity for $A \geqslant 0$, $\mathrm{Im}t_{ij} = \rho \sum_k t_{ik} t^*_{jk}$.

IV. UNCOUPLED $^1S_0$ WAVE

This section is devoted to the study of the $^1S_0$ partial wave and for the sake of concision I follow the convention, also applied to any other partial wave, that whenever DRs already used in Ref. [44] are also employed here, they are not written again and the interested reader is referred to Ref. [44]. One can also deduce the corresponding expression from the general formalism described in Sec. II.

The case with only one-subtracted DRs [44] is discussed first, because one can then study the interesting long-range correlations between the effective range and scattering length for the $^1S_0$ partial wave, first noticed in Ref. [35] and also derived in the NLO N/D study of Ref. [44].[13] The unique free parameter in this case, ν_1, is fixed in terms of the $^1S_0$ scattering length a_s,

$$\nu_1 = -\frac{4\pi a_s}{m}, \tag{25}$$

with the experimental value $a_s = -23.76 \pm 0.01$ fm [33], which is much larger in absolute value than $1/M_\pi$. The large value for ν_1 corresponding to Eq. (25) is given in Table III and is a large number in units of M_π^{-1} (in these units $4\pi/m \simeq 1.85$). At this point it is worth stressing that the power counting for the subtraction constants ν_i is based on the change of the subtraction point along the LHC [Eq. (19)]. This cut is absent when pions are integrated out and this is why this large value for ν_1, owing to the scattering length, cannot be foreseen by the offered chiral counting. I have explicitly checked that $D(A)$ in the low-energy region along the LHC, which fixes the power counting for the subtraction constants Eq. (24), is enhanced by around one order of magnitude owing to the large value of $|a_s| \gg M_\pi^{-1}$. However, let us notice that this enhancement just induces in the power counting a global additive constant in the chiral power of each subtraction constant [e.g., we could consider in this case that $D(A) = \mathcal{O}(p^{-1})$, in the same way as Ref. [37] considered $a_s \sim \mathcal{O}(p^{-1})$]. Given the fact that only relative chiral powers between subtraction constants matter, this global additive constant does not actually affect my calculations. However, one should stress that ν_1 already appears at LO and its large size is well accounted for by the fact that the method is nonperturbative at any order in the calculation of $\Delta(A)$. Incidentally let us note that ν_1 does not enter in the calculation of $\Delta(A)$.

The phase shifts obtained in this case are shown in Fig. 1 as a function of the c.m. three-momentum, denoted by p ($p = \sqrt{A}$), up to $p = 300$ MeV. I choose this value because it is smaller than the the nearby threshold for one-pion production at around $p = 360$ MeV and the inelastic channel $NN\pi$ is not included. In addition, it is also shown below that the expansion scale $\Lambda \gtrsim 3M_\pi$, so that larger values of p are too close to Λ. This is also the same range of energies taken in previous studies to show the results of NN scattering from ChPT and DRs [42–44]. The (red) hatched area corresponds to the results with $\Delta(A)$ calculated up to and including $\mathcal{O}(p^3)$ contributions

[13]The correlation between the effective range and the scattering length in Eq. (27) was derived earlier in atomic physics for Van der Waals potentials [76] and thoroughly confronted with data [77].

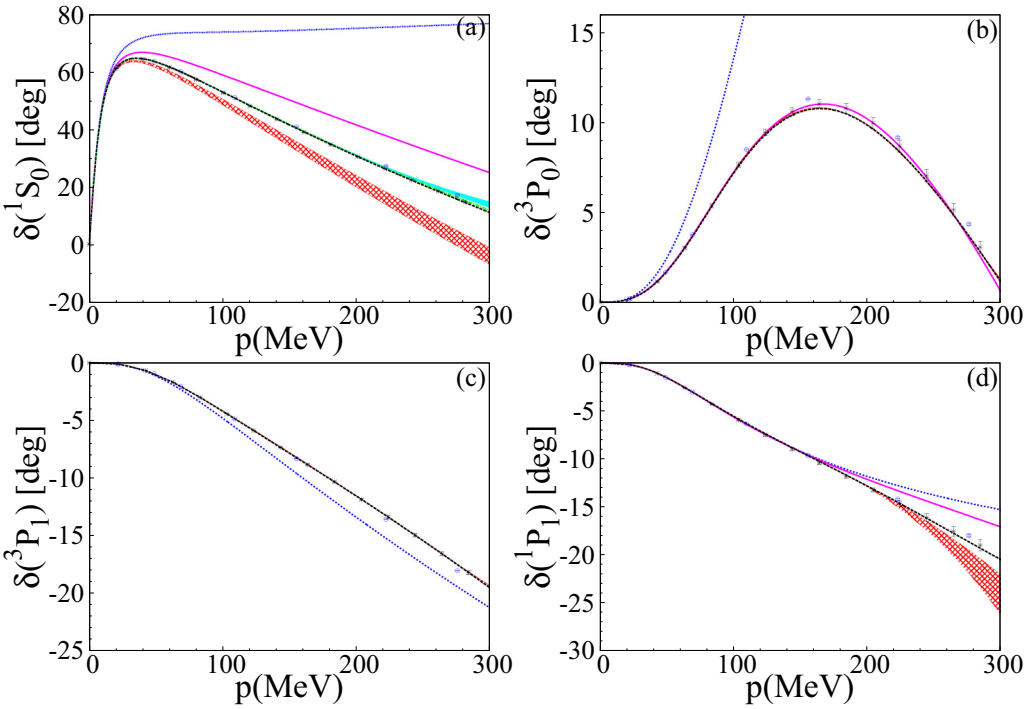

FIG. 1. Phase shifts of $^1S_0$ (a) and uncoupled P waves (b)–(d). Once-subtracted DR results: NNLO (red hatched areas), NLO [44] (magenta solid lines). Twice-subtracted DR results: NNLO (cyan band), NLO [44] (green dash-dotted line). P waves: NNLO (red hatched areas), NLO (magenta solid lines). In all the panels, OPE or LO results [42] are the blue dotted lines. The results obtained are compared with (i) the PWA93 phase shifts [47] (black dashed lines); the mean between the phase shifts from PWA93 [47] and the potential models Nijm2, Reid93 [58], and AV18 [59] (black asterisks); (iii) phase shifts with error bars of the PWA of Ref. [60] (blue open circles).

and by taking into account the variation in the results from the different values employed for the NLO πN ChPT counterterms in Table I. Together with the present outcomes I also show the once-subtracted results of Ref. [42], which only includes OPE (blue dotted line), and the NLO results of Ref. [44] (magenta solid line). The phase shifts obtained are always compared with the results from the neutron-proton (np) PWA93 [47] (black dashed line), and the mean of the latter and the phases obtained with the potentials Nijm2, Reid93 [58], and AV18 [59] (black asterisks). The error is estimated in this case from the variance of the set of values. I also show the recent PWA of Ref. [60] that provides errors by the (blue) open circles. It is interesting to remark that the $^1S_0$ phase shifts are better reproduced for lower energies at NNLO than at smaller orders, though one still observes an excess of repulsion.

Next let us calculate the effective range expansion (ERE) parameters for the $^1S_0$ by taking into account the relation

$$\frac{4\pi}{m}\frac{D}{N} = -\frac{1}{a_s} + \frac{1}{2}r_s A + \sum_{i=2}^{6} v_i A^i - i\sqrt{A} + \mathcal{O}(A^7), \quad (26)$$

with r_s the $^1S_0$ effective range and v_i, $i = 2,\ldots,6$ the shape parameters. To evaluate the different ERE parameters I make use of the efficient numerical method developed in the Appendix. The resulting values for r_s and the shape parameters v_i, $i = 2,\ldots,6$, are given in Table II in the second and third rows for NLO and NNLO, respectively. The latter are indicated by NNLO-I. These results are compared with the ones from the calculation based on the NNLO *NN* potential of Refs. [33] and [50], and with the PWA93 values. The results

TABLE II. Values for effective range r_s (fm) and the shape parameters v_i, $i = 2,\ldots,6$ in units of fm^{2i-1} for the present results at NNLO with once-subtracted DRs (NNLO-I, third row) and twice-subtracted DRs (NNLO-II, fourth row). The results at NLO with once-subtracted DRs (second row), the outcomes from the NNLO *NN* potential in Refs. [33,50] (fifth and sixth rows, respectively), and the values for PWA93 [47] obtained in Refs. [33,50] (last row) are also given.

	r_s	v_2	v_3	v_4	v_5	v_6
NLO	2.32	−1.08	6.3	−36.2	225	–1463
NNLO-I	2.92(6)	−0.32(8)	4.9(1)	−27.7(8)	177(4)	–1167(30)
NNLO-II	2.699(4)	−0.657(3)	5.20(2)	−30.39(9)	191.9(6)	–1263(3)
Ref. [33]	2.68	−0.61	5.1	−30.0		
Ref. [50]	2.62 to 2.67	−0.52 to −0.48	4.0 to 4.2	−20.5 to −19.9		
Ref. [47]	2.68	−0.48	4.0	−20.0		

TABLE III. The partial wave, the type of DRs employed to study it and the values for the free parameters involved are given in columns from left to right. The notation already introduced in Ref. [44] is followed here. Then, mDR, with $m = 1,2,\ldots$, corresponds to m-times-subtracted DRs and for the higher NN partial waves the abbreviation LTS is used to indicate that ℓ (or J for the mixing partial waves) subtractions are taken to satisfy the threshold behavior, following the standard formalism explained in Sec. II C. The units are given by appropriate powers of M_π^2, although they are not explicitly shown. The intervals in the values given for the parameters include the variation in the sets of values for the c_i's.

Wave	Type of DRs	Parameters
$^1S_0$	1DR	$\nu_1 = 30.69$
	2DR	$\nu_1 = 30.69$, $\nu_2 = -23(1)$, $\delta_2 = -8.0(3)$
$^3P_0$	3DR	$\nu_2 = 1.644$, $\delta_2 = 2.82(5)$, $\delta_3 = 0.18(6)$
$^3P_1$	3DR	$\nu_2 = -1.003$, $\delta_2 = 2.7(1)$, $\delta_3 = 0.47(3)$
$^1P_1$	2DR	$\nu_2 = -1.723$, $\delta_2 = 0.4(1)$
$^1D_2$	LTS	$D^{(1)}(0) = 0.07(1)$
$^3D_2$	LTS	$D^{(1)}(0) = -0.017(3)$
$^1F_3$	LTS	$D^{(2)}(0) = 0.057(3)$
$^3F_3$	LTS	$D^{(2)}(0) = 0.035(5)$
$^1G_4$	LTS	$D^{(3)}(0) = -0.014(2)$
$^3G_4$	LTS	$D^{(3)}(0) = -0.055(5)$
$^1H_5$	LTS	$D^{(4)}(0) = 0.156$
$^3H_5$	LTS	$D^{(4)}(0) = 0.066$
$^3S_1$-$^3D_1$	1DR $^3S_1$, 2DR $^3D_1$, mixing	E_d
	2DR all	a_t, r_t, E_d
	2DR $^3S_1$, mixing, 3DR $^3D_1$	a_t, r_t, E_d, $\nu_3^{(22)} = -2.05(5)$
$^3P_2$-$^3F_2$	3DR for $^3P_2$ and LTS for the others	$\nu_2^{(11)} = 0.178$, $D_{11}^{(1)}(-M_\pi^2) = 0.025(5)$, $\nu_3^{(11)} = 0.155(5)$ $D_{22}^{(1)}(-M_\pi^2) = 0.011(4)$
$^3D_3$-$^3G_3$	LTS	$D_{11}(-M_\pi^2) = 0.90(5)$, $D_{22}^{(2)}(-M_\pi^2) = -0.09(1)$
$^3F_4$-$^3H_4$	LTS	$D_{11}^{(1)}(-M_\pi^2) = -0.009(3)$

for v_3 and v_4 are very similar to those obtained in Ref. [33]. The difference between Refs. [33] and [50] stems from the fact that in the latter reference SFR is used, instead of dimensional regularization. One also observes a clear improvement in the reproduction of the ERE parameters from NLO to NNLO. At NLO the errors in Table II reflect the numerical uncertainty in the calculation of higher-order derivatives, while at NNLO they take into account additionally the spread in the results from the different sets of c_i's used.

In the once-subtracted case a power series expansion of the ERE parameters can be worked out as a function of a_s, as it was done previously for r_s in Ref. [44] at NLO, to which I refer for further details. In this way, the ERE parameters are given by the expansions

$$r_s = \alpha_0 + \frac{\alpha_{-1}}{a_s} + \frac{\alpha_{-2}}{a_s^2},$$
$$v_n = \sum_{m=-n-1}^{0} \frac{v_n^{(m)}}{a_s^m}, \tag{27}$$

with the coefficients α_i and $v_n^{(i)}$ independent of a_s. The values of of α_i ($i = -2,-1,0$) at NNLO are

$$\alpha_0 = 2.61 \text{ to } 2.73 \text{ fm},$$
$$\alpha_{-1} = -5.93 \text{ to } -5.65 \text{ fm}^2, \tag{28}$$
$$\alpha_{-2} = 5.92 \text{ to } 6.12 \text{ fm}^3.$$

These figures are perfectly compatible with those obtained in the first entry of Ref. [35], $\alpha_0 = 2.59$ to 2.67 fm, $\alpha_{-1} = -5.85$ to -5.64 fm^2 and $\alpha_{-2} = 5.95$ to 6.09 fm^3. This reference employs the chiral NN potential in a Schrödinger equation that is renormalized with an energy-independent boundary condition. In the present case, the expansions in Eq. (27) are consequences of basic principles of a NN partial wave like unitarity, analyticity, and chiral symmetry. The resulting phase shifts obtained here, shown by the (red) hatched area in Fig. 1, are also coincident with those obtained by Ref. [35]. They are rather similar as well to the ones obtained by employing only one contact term in the third entry of Ref. [38].

Next, I consider the twice-subtracted DRs [44]. The subtraction constant ν_1 is given by Eq. (25), while ν_2 and δ_2 are directly fitted to the np PWA93 phase shifts.[14] The best fitted values are shown in Table III, where, for each partial wave (first column), the values of the free parameters are given in the last column according to the type of DRs employed (second column). The uncertainty in the given value of a subtraction constant takes into account the spread in the results that stem from the variation of the c_i's taken from Table III.

As shown by the (cyan) shaded area in Fig. 1 it is clear that the reproduction of data is very good; indeed, it lies on top of the PWA93 np phase shifts. In the same figure I show

[14]Because Ref. [47] does not provide errors, I always perform a least square fit, without weighting.

by the (green) dash-dotted line the twice-subtracted DR result at NLO, which reproduces the Nijmegen data equally well as obtained at NNLO, with the fitted values $\nu_2 = -11.9 M_\pi^{-4}$ and $\delta_2 = -4.6 M_\pi^{-2}$. The resulting ERE shape parameters are shown in the fourth row of Table II, where one observes a remarkable good agreement with Ref. [33]. I predict $r_s = 2.70$ fm, which is compatible with its experimental value $r_s = 2.75 \pm 0.05$ fm [33]. The $^1S_0$ phase shifts are also well reproduced in terms of two free parameters in the dispersive study of Ref. [51].

The value of ν_2 in Table III is rather large, a 25% smaller in absolute value than $\nu_1 \simeq 31 M_\pi^{-2}$ [Eq. (25)]. By reshuffling the once-subtracted DR in the form of a twice-subtracted DR, one can predict the value for the subtraction constant ν_2, that I denote by $\nu_2^{\rm pred}$. It is given by the expression

$$\nu_2^{\rm pred} = \frac{1}{\pi} \int_{-\infty}^{L} dk^2 \frac{\Delta(k^2) D(k^2)}{(k^2)^2}, \tag{29}$$

with the numerical value $\nu_2^{\rm pred} \simeq -6.0$, -6.4, and $-7.5 \pm 0.2 M_\pi^{-4}$ when $\Delta(A)$ is calculated up to $\mathcal{O}(p^0)$, $\mathcal{O}(p^2)$, and $\mathcal{O}(p^3)$, respectively. The difference between the predicted and fitted values for ν_2 at NLO is denoted by $\delta\nu_2^{(0)}$. The superscript takes into account the chiral order for ν_2, $\mathcal{O}(p^{-2+m})$ [Eq. (24)]. The value obtained is $\delta\nu_2^{(0)} \simeq -5.5 M_\pi^{-4}$. At NNLO, to calculate $\delta\nu_2^{(1)}$ one has to subtract $\delta\nu_2^{(0)}$ to the difference between the fitted value in Table III and the predicted one from Eq. (29). Then it results that $\delta\nu_2^{(1)} \simeq -15 + 5.5 = -9.5 M_\pi^{-4}$. This implies that to overcome the excess of repulsion at NNLO, one needs to incorporate a significant contribution from short-distance physics to give account of "missing physics," beyond the pure long-range contributions[15] that stem from the once-subtracted DR case and that are not able to provide an accurate reproduction of data; cf. Fig. 1. The large value for $\delta\nu_2^{(1)}$ is mainly attributable to the $\mathcal{O}(p^2)$ πN counterterms c_i's, which, in turn, are dominated by the $\Delta(1232)$ resonance contribution [12,78]. This can be easily seen by performing a fit to data in which one sets $c_i = 0$ for all of them. A good reproduction of the PWA93 phase shifts results, but now $\delta\nu_2^{(1)} \simeq -1.5 M_\pi^{-4}$, which is much smaller than $\delta\nu_2^{(0)}$, with a ratio $\delta\nu_2^{(1)}/\delta\nu_2^{(0)} \sim 30\% \sim \mathcal{O}(p)$. This indicates that once the large contributions that stem from the c_i coefficients are discounted a quite natural (baryon) chiral expansion emerges. From the previous ratio one also learns that the expansion scale Λ is such that $M_\pi/\Lambda \gtrsim 1/3$.

Let us consider now the relevance of the different contributions to $\Delta(A)$ by following the same procedure as in Ref. [44], so that the last integral in the r.h.s. of Eq. (6) is evaluated for $n = 2$ with the full function $D(A)$ fitted to data, but with $\Delta(A)$ evaluated with only some contributions or all of them. The result of this exercise is given in Fig. 2(a) for the c_i coefficients of Ref. [69] (second row of Table I). The (black) dash-dotted line corresponds to OPE, the (blue) dotted line takes into account the full $\mathcal{O}(p^2)$ TPE, including both two-nucleon reducible and irreducible TPE, and the (cyan) double-dotted line contains the $\mathcal{O}(p^3)$ two-nucleon irreducible TPE [46]. Finally, the (red) solid line results by keeping all the contributions to $\Delta(A)$, and it is clear that that the $\mathcal{O}(p^3)$ irreducible TPE is the largest subleading contribution. In addition, $\Delta(A)$ is also shown along the LHC in Fig. 2(b), where each line included has the same meaning as in the right panel although for $\Delta(A)$ the (cyan) shaded area reflects the variation in the $\mathcal{O}(p^3)$ irreducible TPE contribution by varying between the different sets of c_i's considered, as discussed above. This band indicates a large source of uncertainty in $\Delta(A)$.

The increase in energy of the relative size of the subleading TPE contribution should be expected because at low energies the suppression mechanism owing to the earlier onset of the OPE source of $\Delta(A)$ along the LHC at L is more efficient. In addition, it is well-known that the $\Delta(1232)$ plays a prominent role in πN scattering, which manifests in the large size of the LECs c_3 and c_4 in Table I [12,78]. Once the leading effects of including the $\Delta(1232)$ are taken into account at $\mathcal{O}(p^3)$ the chiral expansion stabilizes [32,50], as it was also concluded above. From now on, I skip the discussion on the relative importance of the different contributions to $\Delta(A)$ for those NN partial waves with a similar behavior as the $^1S_0$.

V. UNCOUPLED P WAVES

In this section the application of the method to the uncoupled P waves is discussed. At NNLO one has for these waves that

$$\lambda_P = \lim_{A\to-\infty} \frac{\Delta(A)}{(-A)^{(3/2)}} > 0, \tag{30}$$

so that, according to the results of Ref. [44], its Proposition 4, a once-subtracted DR for $D(A)$ [Eq. (4)] does not converge and more subtractions should be taken. Then let us consider the twice- and three-times-subtracted DRs. The twice-subtracted DRs is of the same form as the one given in Ref. [44] for the $^3P_0$ wave; hence, I write here explicitly only the three-times-subtracted DRs that are used in slightly different form compared with Ref. [44],

$$\begin{aligned} D(A) &= 1 + \delta_2 A + \delta_3 A\left(A + M_\pi^2\right) \\ &\quad + \left(\nu_2 - \nu_3 M_\pi^2\right) A \left(A + M_\pi^2\right)^2 \frac{\partial g\left(A, -M_\pi^2\right)}{\partial M_\pi^2} \\ &\quad - \nu_3 A\left(A + M_\pi^2\right)^2 g\left(A, -M_\pi^2\right) + \frac{A\left(A + M_\pi^2\right)^2}{\pi} \\ &\quad \times \int_{-\infty}^{L} dk^2 \frac{\Delta(k^2) D(k^2)}{(k^2)^3} g\left(A, k^2, -M_\pi^2; 2\right), \\ N(A) &= \nu_2 A + \nu_3 A^2 + \frac{A^3}{\pi} \int_{-\infty}^{L} dk^2 \frac{\Delta(k^2) D(k^2)}{(k^2 - A)(k^2)^3}. \end{aligned} \tag{31}$$

Here all the subtractions in $N(A)$ and one in $D(A)$ are taken at $C = 0$, while the other two subtractions in $D(A)$ are at $C = -M_\pi^2$. This is done to avoid handling an infrared diverging integral along the RHC multiplying ν_2 that would result if all the subtractions were taken at $C = 0$. The function

[15] This is meant here as the physics driven by the multipion exchanges giving rise to the LHC and to $\Delta(A)$.

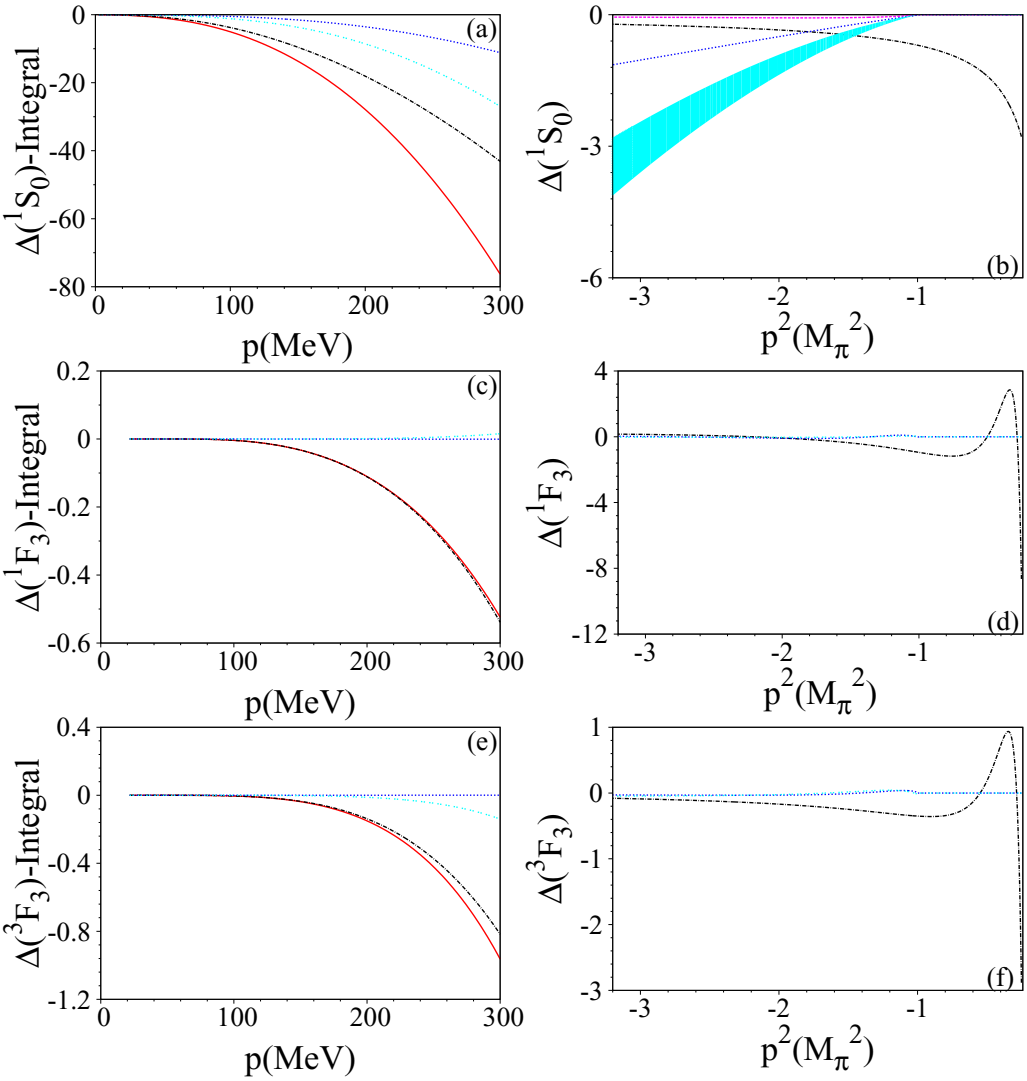

FIG. 2. The left panels quantify the different contributions to the double-dispersive integrals in the DRs employed to calculate $D(A)$, and the right panels correspond to the different contributions to $\Delta(A)$ along the LHC. (a),(b) $^1S_0$; (c),(d) $^1F_3$; and (e),(f) $^3F_3$. For the precise meaning of the lines, the reader is referred to the text.

$g(A,k^2,C;m)$ in Eq. (31) is defined as

$$g(A,k^2,C;m) = \int_0^\infty dq^2 \frac{\rho(q^2)(q^2)^m}{(q^2-A)(q^2-k^2)(q^2-C)^m}, \tag{32}$$

which can be worked out algebraically and written as a linear combination of functions $g(x,y)$ [Eq. (7)]. In all the cases the subtraction constant ν_2 is fixed in terms of the scattering volume, a_V,

$$\nu_2 = 4\pi a_V/m. \tag{33}$$

For a_V the values $0.890M_\pi^{-3}$, $-0.543M_\pi^{-3}$, and $-0.939M_\pi^{-3}$ are employed for the partial waves $^3P_0$, $^3P_1$, and $^1P_1$, in order, as deduced from Ref. [47].

For the $^3P_0$ wave the twice-subtracted DRs at NNLO do not provide stable results under the increase in absolute value of the lower limit of integration along the LHC. However, the three-times-subtracted DRs are convergent. Notice that, as discussed in Sec. III B, on top of the number of subtractions required by the chiral counting one needs to have well-defined IEs; otherwise, the very same power counting does not make sense. Regarding the subtraction constants ν_3, δ_2, and δ_3 in Eq. (31), one can fix $\nu_3 = 0$ because it plays a negligible role in the fits and, if released, the fit is stable. The fitted values for δ_2 and δ_3 are collected in Table III. The phase shifts calculated, shown in panel (b) of Fig. 1 by the (red) hatched area, reproduce exactly the PWA93 phase shifts [47]. The results with different sets of values for the c_i counterterms cannot be distinguished either between each other. I have also checked that a three-times-subtracted DR at LO and NLO provides already a prefect reproduction of data as well. Then the wave $^3P_0$ studied at $\mathcal{O}(p^3)$ is not a good partial wave to learn above chiral dynamics, because, independently of the

order up to which $\Delta(A)$ is calculated, the reproduction of data is excellent when three subtractions are taken.

The situation is completely analogous for the wave $^3P_1$ and the fitted values of the parameters can be read from Table III. The resulting phase shifts are shown in the panel (c) of Fig. 1, which again reproduce perfectly the PWA93 phase shifts, independently of the set of values for the c_i's chosen in Table I. At NLO [44] it is also necessary to take three-times subtracted DRs so as to obtain stable results, and the reproduction of data is equally perfect.

For the $^1P_1$ partial wave the twice-subtracted DR results are quite stable at low energies. The parameter δ_2 is fitted to the PWA93 phase shifts and given in Table III. I show the results in panel (d) of Fig. 1, where the curves obtained with the c_i from Ref. [11], by reproducing the πN phase shifts with Lorentz covariant EOMS ChPT, are the closest to data. The improvement in the reproduction of data for the $^1P_1$ partial wave by the twice-subtracted DRs at NNLO compared with the results obtained at NLO with the same number of subtractions (magenta solid line) is a significant effect from πN physics.

Because of the truncation of the LHC integrals in Ref. [51] for $A < -9M_\pi^2/4$ this reference is not sensitive to the high-energy behavior of $\Delta(A)$, and in particular to λ_P, Eq. (30). As a result Ref. [51] can obtain phase shifts for the uncoupled P waves with only one free parameter, which also reproduce the experimental phase shifts rather closely.

VI. UNCOUPLED D WAVES

The function $\Delta(A)$ for the uncoupled D waves has the asymptotic behavior

$$\lambda_D = \lim_{A\to-\infty} \frac{\Delta(A)}{(-A)^{3/2}} < 0, \tag{34}$$

and with this sign the resulting IE from the twice-subtracted DRs [44] is convergent. The only free parameter per partial wave is $\delta_2 = D^{(1)}(0)$, which is fitted to the PWA93 phase shifts and its value is given in Table III. The reproduction of data is excellent, as shown by the (red) hatched areas in Figs. 3(a) and 3(b), where the left panels correspond to the singlet waves and the right ones to the triplet waves. The results obtained indeed overlap the PWA93 phase shifts. One can see a remarkable improvement from NLO to NNLO owing to the inclusion of NLO πN dynamics (without any further free parameter). In the $^1D_2$ partial wave this occurs in the whole energy range shown, while for the $^3D_2$ it takes place in the higher part, above $p \gtrsim 220$ MeV. The perturbative one-loop ChPT phase shifts [46] are also shown in Fig. 3 by the (cyan) shaded areas. These curves are quite different from the full results given by the hatched areas, which clearly indicates that the perturbative treatment of the NN D waves is not accurate.

VII. UNCOUPLED F WAVES

For the F waves one has three subtractions with two free parameters δ_2 and δ_3. I fix $\delta_2 = 0$ in the following (according to the principle of maximal smoothness) and fit δ_3 to data, which is related to $D^{(2)}(0)$ in virtue of Eq. (13), with the fitted value given in Table III. The NNLO results are shown by the (red) hatched areas in Figs. 3(c) and 3(d). One observes an improvement compared to the NLO results in the reproduction of data for the wave $^3F_3$ and momenta somewhat above 200 MeV. For the wave $^1F_3$ the NNLO outcomes are very similar to those obtained at lower orders and show a small discrepancy with the PWA93 phase shifts [47] for $p > 150$ MeV. However, the results in this case run very close to the high-quality AV18 potential [58], which determines the lower end of the error bars attached to the bursts and to the recent PWA of Ref. [60]. Thus, the failure reported in Refs. [33,50] to reproduce simultaneously the D and F waves by using the NNLO chiral potential calculated in dimensional regularization in Ref. [46], because of the large values of the c_i counterterms, does not happen within the approach used here. The dependence on the precise set of values taken for the c_i's from πN scattering is quite mild for the full results and gives rise to a modest uncertainty band. Indeed, the calculation at NNLO describes the PWA93 phase shifts for the D and F waves better than the NLO ones [44], without increasing the number of subtractions, which is not the case for all of these waves in Ref. [33] based on the (modified) Weinberg approach when comparing their NLO and NNLO results. Recently, Ref. [79] arrived at similar conclusions by regularizing the Lippmann-Schwinger equation in partial waves with a new type of local cutoff function that does not distort the analytical properties of the NN potential along the real axis[16] in a given partial wave. Within the theory employed here, the right analytical properties of the NN partial waves in the whole complex A plane are accomplished by construction.

One also observes that for the F waves the one-loop ChPT perturbative phase shifts [46] run much closer to the full results than for the D waves, which clearly indicates that F waves are more perturbative. Nevertheless, the relative deviation of the phase shifts in the pure perturbative ChPT calculation compared with the full solution is still around 50% at the end of the interval shown in Fig. 3. However, the situation is not so dramatic when considering the actual expansion followed in the present work. The phase shift at $p = 300$ MeV for the $^3F_3$ has the values, at the different orders, of -3.5 (LO), -2.8 (NLO), and -2.2(NNLO) degrees. Thus, the relative deviation with respect to the NNLO result clearly decreases by increasing the order of the calculation, so that at LO it is around 50%, but at NLO it is reduced to around 20%. A similar conclusion on the more perturbative nature of the F waves was also reached in the one-loop ChPT calculation of Ref. [46] by comparing with experimental data.

It is also interesting to remark from Fig. 3 that the widths of the (cyan) shaded bands for the perturbative results [46] reflect a much larger dependence on the c_i coefficients than the one corresponding to the full nonperturbative results given by the (red) hatched areas. This is a twofold effect. On the one hand, the nonperturbative method reduces the sensitivity on the precise values of the c_i's employed for most of the partial waves and, on the other hand, refitting the subtraction constants for each set of c_i's employed further reduces the dependence on them.

[16] It does, however, in the complex A plane.

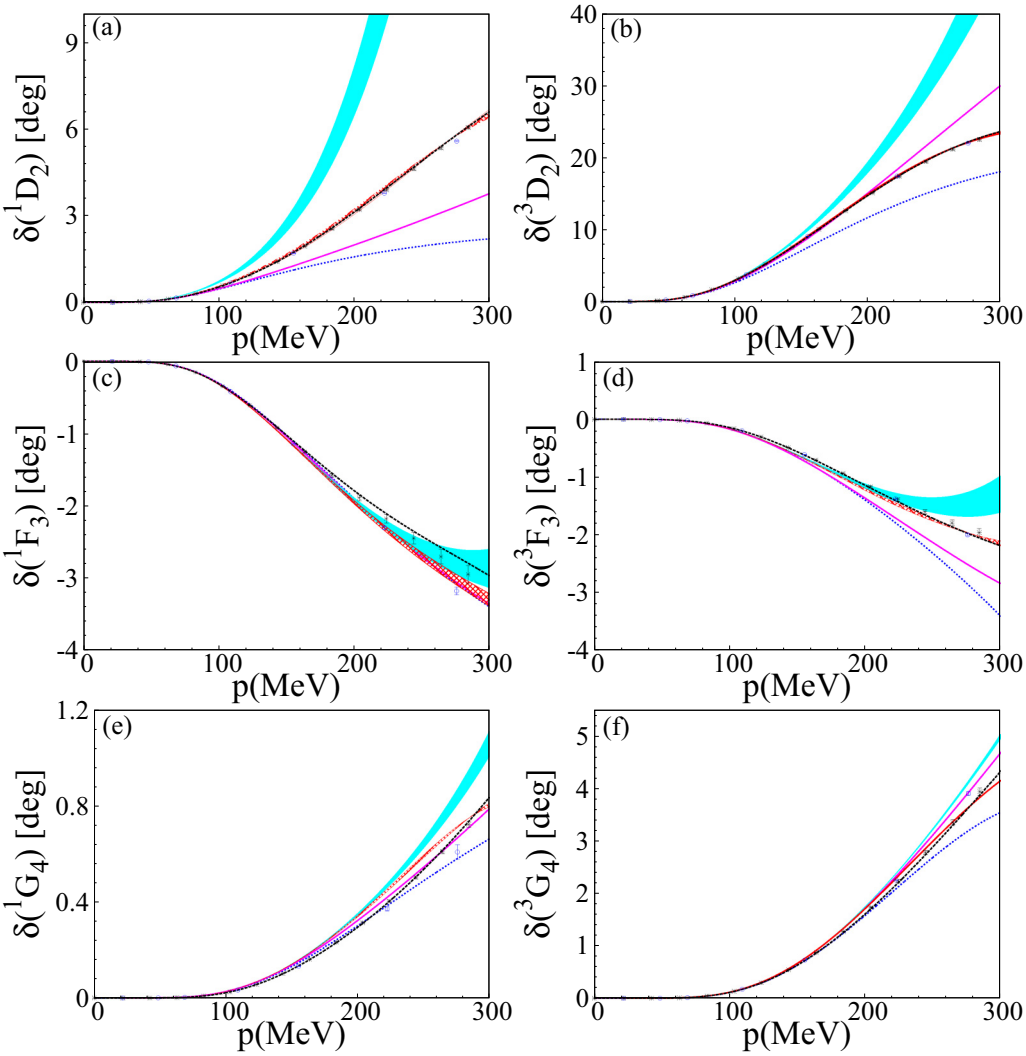

FIG. 3. The phase shifts for D and higher partial waves are plotted. The meaning of the lines is the same as in the last three panels of Fig. 1, though the number of subtraction taken is given by the standard formalism for higher partial waves; cf. Sec. II C. In addition, perturbative phase shifts [46] are also shown by the (cyan) shaded bands.

The increase in the perturbative character of the F waves can also be seen by considering the relevance of the different contributions of $\Delta(A)$ to the integral on the r.h.s. of Eq. (11), proceeding in a similar way to that followed for the $^1S_0$ partial wave in Sec. IV. The result is shown in Figs. 2(c) and 2(e), where the second row corresponds to $^1F_3$ and the third one to $^3F_3$. In the right panels the different contributions to $\Delta(A)$ along the LHC are plotted. The meanings of the lines here are the same as for the $^1S_0$ wave, though now the c_i's are taken from Ref. [11], given in the last row of Table I, which is enough for the present purposes. Notice that for the F waves a qualitative different situation is found with respect to what is shown for the $^1S_0$ (that also holds for the P and D waves). For the F and higher waves the subleading two-nucleon irreducible TPE contribution is much less important and OPE is, by far, the dominant contribution, as it should correspond to a perturbative high-ℓ wave.

VIII. UNCOUPLED G WAVES

For the uncoupled G waves, $^1G_4$ and $^3G_4$, one has four subtractions, of which δ_i ($i = 2,3,4$) are free but, according to the principle of maximal smoothness, all of them are fixed to 0 except $\delta_4 = D^{(3)}(0)/3!$, which is fitted to data, with its value given in Table III. The corresponding results are shown by the (red) hatched areas in Figs. 3(e) and 3(f). For both partial waves the actual dependence on the c_i coefficients in the resulting phase shifts is almost negligible and the hatched areas degenerate to lines. The low-energy results are very similar at NLO and NNLO and reproduce the PWA93 phase shifts quite well. These results are better than the perturbative ones, given by the (cyan) shaded areas. As indicated for the uncoupled F waves, here OPE overwhelmingly dominates the different contribution to the dispersive integral on the r.h.s. of Eq. (11). This indicates that these waves are rather perturbative, though still one observe differences around 30% for $p \lesssim 300$ MeV

in the corresponding panels of Fig. 3 between the full and the perturbative results.

IX. UNCOUPLED H WAVES

The uncoupled H waves, $^1H_5$ and $^3H_5$, require five-times-subtracted DRs with $\ell = 5$ in Eqs. (11) and (12). I fit $\delta_5 = D^{(4)}(0)/4!$ to the PWA93 phase shifts, while $\delta_{2,3,4}$ are fixed to 0 (principle of maximal smoothness). The fitted values are given in Table III, and the resulting fit is stable if δ_i $(i = 2,3,4)$ are released. The PWA93 phase shifts for $J \geqslant 5$ correspond to those obtained from the NN potential model of Ref. [80], so I do not plot them here or the resulting phase shifts. One can notice that the phase shifts in one-loop ChPT [46] run very close to the full results, particularly for the $^3H_5$, in which case both are coincident. This clearly indicates the perturbative nature for the H waves. In connection with this, the dependence of the results on the c_i's is negligible.

I have included these waves under consideration because I find it interesting to discuss in this case the behavior of the function $N(A)$ compared with its perturbative solution in powers of $\Delta(A)$. The point is that for a weak interaction [small $\Delta(A)$ at low three-momentum] one can expect that $D(A) \simeq 1$ at low energies. It is then reasonable to consider that substituting $D(A) \to 1$ in the integral on the r.h.s. of Eq. (12) would be meaningful in calculating $N(A)$ at low energies, because one has a rapid converging integral owing to the factor $(k^2)^\ell$ in the denominator for a sufficiently large value of ℓ. The leading perturbative result for $N(A)$ in powers of $\Delta(A)$, denoted by $N_p(A)$, is then

$$N_p(A) = \frac{A^\ell}{\pi}\int_{-\infty}^{L} dk^2 \frac{\Delta(k^2)}{(k^2)^\ell (k^2 - A)}. \tag{35}$$

I consider only the $^3H_5$ wave, but a similar discussion would follow for $^1H_5$ as well. In Fig. 4(a) I show by the (red) solid line the full $N(A)$ and by the (blue) dashed line the perturbative result $N_p(A)$. One sees that they are very similar, as expected for a partial wave with an ℓ as high as 5. In Fig. 4(b) the real part of $D(A)$ from Eq. (11) is drawn, which is very close to 1, as discussed. All these curves are obtained by employing the c_i's from Ref. [11]. A bit higher in energy both $N_p(A)$ and $N(A)$ have a zero at around $\sqrt{A} = 450$ MeV. Because $T(A) = N(A)/D(A)$ this would imply that $T(A) = 0$ there, unless $D(A)$ is also zero at the same point. This is indeed the case and it is is the reason why $D(A)$ starts to decrease for $\sqrt{A} > 200$ MeV in Fig. 4.

Another question of interest to think about is what has been gained by solving exactly Eq. (11) instead of using only the perturbative solution, Eq. (35), or the pure perturbative ChPT one-loop calculation [46], or even the Born approximation. The main point is that by solving the full and nonperturbative Eq. (11) one can then state that Eq. (35) is a perturbation of a well-defined and existing nonperturbative solution. By solving exactly Eq. (11) one needs to consider explicitly δ_5 as a free parameter for the uncoupled H waves. As a matter of fact, δ_5 is not only necessary for a good fit, but it is also required to keep $D(A) \simeq 1$ at low three-momentum. Otherwise, the contribution from the dispersive integral of $D(A)$ on the r.h.s. of Eq. (12) would be too large and negative and would render a too-strong function $N(A)$ in plain disagreement with $N_p(A)$.

X. COUPLED $^3S_1$-$^3D_1$ WAVES

Let us start the study of the $^3S_1$-$^3D_1$ coupled-partial-wave system in terms of just one free parameter, which corresponds to the pole position of the deuteron in the A-complex plane, $k_d^2 = -mE_d$, with $E_d = 2.225$ MeV the deuteron binding energy. The aim here is to consider the long-range correlations first noticed in Ref. [35] for NN S waves. Thus, one proceeds similarly to that given in Ref. [44], with the only difference that now the subtraction constant $\nu_1^{(11)}$ is fixed to reproduce the experimental deuteron pole position, while in Ref. [44] it was fixed to the experimental triplet scattering length. This is why I write here the DRs considered for the $^3S_1$,

$$\begin{aligned} D_{11}(A) &= 1 - \frac{A}{k_d^2}\frac{g_{11}(A,0)}{g_{11}(k_d^2,0)} + \frac{A}{\pi}\int_{-\infty}^{L} dk^2 \frac{\Delta_{11}(k^2)D_{11}(k^2)}{k^2} \\ &\quad \times \left[g_{11}(A,k^2) - g_{11}(A,0)\frac{g_{11}(k_d^2,k^2)}{g_{11}(k_d^2,0)} \right], \\ N_{11}(A) &= \nu_1^{(11)} + \frac{A}{\pi}\int_{-\infty}^{L} dk^2 \frac{\Delta_{11}(k^2)D_{11}(k^2)}{k^2(k^2 - A)}, \end{aligned} \tag{36}$$

with all the subtractions taken at $A = 0$. The new function $g_{ij}(A)$ was already given in Ref. [35] and ν_1 in $N_{11}(A)$ is fixed

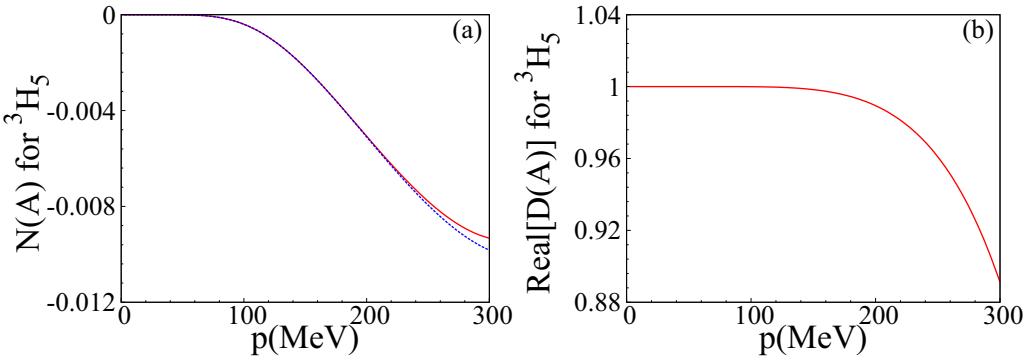

FIG. 4. The functions $N(A)$ and $N_p(A)$ are shown by the (red) solid and (blue) dashed lines in (a), respectively. The real part of the function $D(A)$ is plotted in (b).

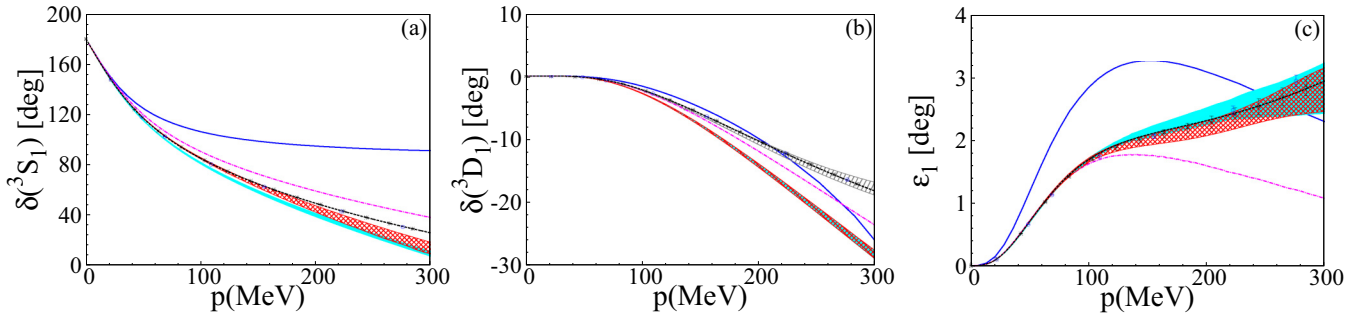

FIG. 5. Phase shifts for (a) ${}^3S_1$, (b) ${}^3D_1$, and (c) the mixing angle ε_1. The (cyan) shaded areas correspond to NNLO-I; the hatched areas with (red) crossed lines are the NNLO-II results. In addition, for the ${}^3D_1$ the hatched areas with (gray) parallel lines correspond to the results obtained by employing three-times-subtracted DRs only for the wave ${}^3D_1$. The (magenta) dot-dashed lines are the NLO phases, while the LO ones are given by the (blue) lines. The meaning of the (black) dashed lines and points is the same as in Fig. 1.

by imposing that $D_{11}(k_d^2) = 0$,

$$\nu_1^{(11)} = \frac{1}{k_d^2\, g_{11}\left(k_d^2,0\right)} \times \left[1 + \frac{k_d^2}{\pi}\int_{-\infty}^{L} dk^2 \frac{\Delta_{11}(k^2) D_{11}(k^2)}{k^2} g_{11}\left(k^2,k_d^2\right)\right]. \tag{37}$$

This expression is already implemented in Eq. (36) for $D_{11}(A)$. The results obtained are shown in Fig. 5 by the (cyan) shaded areas. These results are indicated as NNLO-I and all the subtraction constants are fixed in terms of k_d^2, without any other freedom. The width of the bands originates by taking different sets of c_i's from Refs. [11,69] and varying the input in the iterative procedure. The present NNLO calculation reproduces the PWA93 mixing angle ε_1 much better than the NLO results (magenta dot-dashed lines) without further subtractions. This improvement in the description of ε_1 when passing from NLO to NNLO is also seen in Ref. [33] by employing the Weinberg scheme. The ${}^3S_1$ phase shifts are also reproduced better at NNLO than at NLO, while the ${}^3D_1$ is described somewhat worse by the former. The results for the ${}^3S_1$ and ${}^3D_1$ phase shifts are quite similar to those obtained in Ref. [35], but not for ε_1 as the outcome here is closer to PWA93.

One can also predict in this case the ${}^3S_1$ scattering length (a_t) and effective range (r_t). The former is given in terms of $\nu_1^{(11)}$, [Eq. (37)] as $a_t = -m\nu_1^{(11)}/4\pi$. Regarding r_t, one can proceed similarly as discussed in detail in Ref. [44]; see Eq. (92) there, which shows an implicit correlation between r_t and a_t, because $\nu_{11}(A)$ depends nonlinearly on $D_{11}(A)$. Another observable that I also consider is the slope at threshold of ε_1, indicated as a_ε, and defined by

$$a_\varepsilon = \lim_{A\to 0^+} \frac{\sin 2\varepsilon_1}{A^{\frac{3}{2}}} = 1.128 M_\pi^{-3}, \tag{38}$$

where the numerical value is deduced from the PWA93 phase shifts. It is also interesting to diagonalize the ${}^3S_1$-${}^3D_1$ S matrix around the deuteron pole position. For further details, see Refs. [44,81]. This can be done by means of a real orthogonal matrix [81], parametrized in terms of the angle ϵ_1, and the eigenvalues are denoted by S_0 and S_2. The asymptotic D/S ratio of the deuteron, η, can be expressed in terms of ϵ_1 as $\eta = -\tan\epsilon_1$, and the residue of S_0 at the deuteron pole position is denoted by N_p^2, where $N_p^2 = \lim_{A\to k_d^2} (\sqrt{-k_d^2}+i\sqrt{A})S_0$. Next I study the results for the shape parameters of the lowest eigenphase δ_0 (also called ${}^3S_1$ eigenphase) of S_0 that stems from the diagonalization of the S matrix performed in the physical region $A \geqslant 0$,

$$\sqrt{A}\cot\delta_0 = -\frac{1}{a_t} + \frac{1}{2} r_t A + \sum_{i=2}^{6} v_i A^i + \mathcal{O}(A^{11}). \tag{39}$$

It is well known that the shape parameters are a good testing ground for the range of applicability of the underlying EFT [82].

The scattering length and effective range in the previous equation are the same as given above because coupled-wave effects with the ${}^3D_1$ only affects the shape parameters $v_i, i \geqslant 2$. The values obtained at NLO and NNLO for a_t, r_t, η, N_p^2, and a_ε are shown in Table IV in the second and third rows, respectively. One can observe that the numbers at NNLO (indicated

TABLE IV. Values for a_t, r_t, η, N_p^2 and a_ε at NLO (second row) and NNLO-I (third row). The values given in the fourth row (NNLO-II) are obtained once a_t and r_t are fixed to the experimental figures, which is indicated by a star on top of the values. The results from Refs. [33,81] and [33] are also shown in the fifth and sixth rows, respectively.

	a_t [fm]	r_t [fm]	η	N_p^2 [fm^{-1}]	a_ε [M_π^{-3}]
NLO	5.22	1.47	0.0295	0.714	1.372
NNLO-I	5.52(3)	1.89(3)	0.0242(3)	0.818(10)	1.270(9)
NNLO-II	5.5424*	1.759*	0.02535(13)	0.78173(2)	1.293(8)
Ref. [81]	5.4194(20)	1.7536(25)	0.0253(2)	0.7830(15)	
Ref. [33]	5.424	1.753	0.0245		

TABLE V. Values for the shape parameters v_i, $i = 2,\ldots,6$ in units of fm^{2i-1} at NLO (second row) and at NNLO-I (third row). Those values corresponding to NNLO-II are given in the fourth row. The values from Refs. [81] and [33] appear in the fifth and sixth rows, in order.

	v_2	v_3	v_4	v_5	v_6
NLO	−0.10572(12)	0.8818(11)	−5.427(11)	36.73(11)	–259.9(1.1)
NNLO-I	0.157(22)	0.645(9)	−3.41(13)	23.2(8)	–161(6)
NNLO-II	0.0848(4)	0.762(7)	−4.33(2)	29.0(2)	–198(2)
Ref. [81]	0.040(7)	0.673(2)	−3.95(5)	27.0(3)	
Ref. [33]	0.046	0.67	−3.9		

by NNLO-I) are already rather close to those of Ref. [81], obtained from the PWA93 of np data, and Ref. [33]. It is interesting to remark that the value for r_t is a prediction in terms of only one subtraction constant (fixed by the deuteron binding energy) and NN forces stemming from πN physics. This value deviates from experiment $r_t = 1.759 \pm 0.005$ fm [33] around a 10% at NNLO (∼20% at NLO), while the relative experimental error is around 3%. Other determinations for the parameter η, not shown in Table IV, are $\eta = 0.0256(4)$ [83], 0.0271(4) [84], 0.0263(13) [85], and 0.0268(7) [86]. The values for the shape parameters v_i, $i = 2,\ldots,6$, are given in Table V. To my knowledge the shape parameters with $i > 5$ were not calculated before. I detail in the Appendix the numerical method that allows one to perform the appropriate derivatives up to very high orders.[17] One can appreciate the numerical precision in the calculation of the shape parameters by considering the errors in Table V for the NLO results. The errors at NNLO take into account additionally the variation in the results from the different sets of c_i's employed and the dependence in the input for starting the iterative process. I could have also given shape parameters of orders higher than 6 within a numerical precision of less than 1%, but I skip this because its apparent little relevance in practice. By increasing the order of the shape parameter the numerical accuracy only worsens little by little. For example, it is not until v_{10} that the relative numerical error is bigger than 1% (a 1.5%). For the shape parameters with large order, $i \geqslant 5$, their absolute values increase typically as $\mathcal{O}(1/M_\pi)^{2i-1}$, which is the expected behavior for long-range interactions mediated by OPE. It is clear from Table V that the shape parameters v_i, $i = 2,\ldots,5$ predicted by the NNLO-I calculation (third row) are typically closer to the values of Refs. [33,81] than those at NLO (second row). This is a positive feature indicating a well-behaved expansion of the results obtained by applying the N/D method with the discontinuity $\Delta(A)$ expanded in ChPT.

According to the power counting for the subtraction constants [Eq. (24)] at NNLO, it is considered appropriate to take twice-subtracted DRs. Compared to the NNLO-I case, this implies to take into account one more subtraction for $D_{11}(A)$ and $N_{11}(A)$; another one is needed for the function $N_{12}(A)$ in the mixing partial wave, while the DRs for the $^3D_1$ wave are the same. The three parameters for the $^3S_1$ wave are fixed in terms of the experimental values of k_d^2, r_t and a_t. The twice-subtracted DRs taken now for the $^3S_1$ wave are

$$
\begin{aligned}
D_{11}(A) &= 1 - \frac{A}{k_d^2} - \nu_1^{(11)}\, A\big(A-k_d^2\big) g_{11}^{(d)}(A,0;1) - \nu_2^{(11)}\, A\big(A-k_d^2\big) g_{11}\big(A,k_d^2\big) + \frac{A\big(A-k_d^2\big)}{\pi}\int_{-\infty}^{L} dk^2\, \frac{\Delta_{11}(k^2) D_{11}(k^2)}{(k^2)^2}\, g_{11}^{(d)}(A,k^2;2),\\
N_{11}(A) &= \nu_1^{(11)} + \nu_2^{(11)}\, A + \frac{A^2}{\pi}\int_{-\infty}^{L} dk^2\, \frac{\Delta_{11}(k^2) D_{11}(k^2)}{(k^2)^2(k^2-A)},\\
\nu_1^{(11)} &= -\frac{4\pi a_t}{m},\\
\nu_2^{(11)} &= \frac{\nu_1^{(11)}}{\nu_1^{(11)} k_d^2\, g_{11}\big(0,k_d^2\big) - 1}\left\{\frac{1}{k_d^2} + a_t\left[\frac{4k_d^2}{m}\int_0^\infty dq^2\, \frac{\nu_{11}(q^2) - \rho(q^2)}{(q^2)^2\big(q^2-k_d^2\big)} + \frac{1}{\sqrt{-k_d^2}} - \frac{r_t}{2}\right]\right.\\
&\quad \left. + \frac{k_d^2}{\pi}\int_{-\infty}^{L} dk^2\, \frac{\Delta_{11}(k^2) D_{11}(k^2)}{(k^2)^2}\, g_{11}\big(k_d^2,k^2\big)\right\}.
\end{aligned}
\tag{40}
$$

For the mixing partial wave the DRs are

$$
\begin{aligned}
D_{12}(A) &= 1 - \frac{A}{k_d^2} - \nu_2^{(12)} A\big(A-k_d^2\big) g_{12}\big(A,k_d^2\big) + \frac{A\big(A-k_d^2\big)}{\pi}\int_{-\infty}^{L} dk^2\, \frac{\Delta_{12}(k^2) D_{12}(k^2)}{(k^2)^2}\, g_{12}^{(d)}(A,k^2;2),\\
N_{12}(A) &= \nu_2^{(12)} A + \frac{A^2}{\pi}\int_{-\infty}^{L} dk^2\, \frac{\Delta_{12}(k^2) D_{12}(k^2)}{(k^2)^2(k^2-A)}.
\end{aligned}
\tag{41}
$$

[17]For example, in Ref. [81] it is stated that their numerical setup is not precise enough to calculate v_6 and that it already casts doubts about the numerical accuracy for v_5.

The results obtained now are denoted in the following as NNLO-II and correspond to the (red) hatched areas with crossed lines in Fig. 5. It turns out that one cannot obtain a solution of the resulting IE for $D_{12}(A)$ by implementing any arbitrary value for $\nu_2^{(12)}$. Whenever one finds a meaningful solution the obtained value of $a_\varepsilon = m\nu_2^{(12)}/2\pi$ is always in the band $a_\varepsilon \simeq 1.30$–$1.90 M_\pi^{-3}$. Similar values are also found in Ref. [87] by renormalizing the chiral TPE potential with explicit Δ excitations for NN scattering. In my opinion this difficulty to reproduce the value for a_ε that follows from the PWA93 [Eq. (38)] casts doubts on this number. Notice that the calculated values for ε_1 at low momentum, e.g., for $\sqrt{A} \lesssim 100$ MeV, lie on top of the curve for the PWA93 results as shown in panel (c) of Fig. 5 by the coincident hatched and shaded areas that overlap the PWA93 line. The phase shifts and ε_1 are quite similar to the NNLO-I results in terms of just one free parameter. Nevertheless, the $^3S_1$ phase shifts for NNLO-II are closer to the PWA93 ones at lower energies, but the change for this S wave from once- to twice-subtracted DRs is much less notorious than in the case of the partial wave $^1S_0$, discussed in Sec. IV. One can also see in the fourth row of Table IV that the NNLO-II values for η and N_p^2 are compatible with those of Ref. [81], which is quite remarkable. The value for a_ε mentioned above is shown in the last column of the same table. The shape parameters are given in the fourth row of Table V, where one observes a better agreement with the numbers from Ref. [81] for v_4 and v_5 than for v_2 and v_3. The variation of the values between NNLO-I and NNLO-II for the higher-order shape parameters allows one to estimate in a conservative way the systematic uncertainty affecting their calculation.

The results of Ref. [51] for these coupled partial waves at $\mathcal{O}(p^3)$ contain three free parameters like the NNLO-II results, the quality in the reproduction of data being similar as well. I agree with the remark in Ref. [51] about the dominant role in this channel of long-range physics associated with the exchange of pions. Notice the already rather good reproduction of the PWA93 phase shifts by the NNLO-I results, which depend on only one free parameter.

However, I would like to elaborate further on the fact that at NNLO the results for the $^3D_1$ phase shifts do not offer a good reproduction of the PWA93 ones, being even worse than those at NLO. In view of this, let us consider now the influence in the results of including one more subtraction in the DRs for $^3D_1$ with the aim of determining whether this worsening is an effect that could be counterbalanced in a natural way at $\mathcal{O}(p^4)$. In this way the same twice-subtracted DRs for $^3S_1$ and the mixing partial wave, given in Eqs. (40) and (41), respectively, are used while three-times-subtracted DRs are employed for the $^3D_1$. The latter include two additional subtraction constants, $\delta_3^{(22)}$ and $\nu_3^{(22)}$. Considering the results in the system $^3S_1$-$^3D_1$ from the twice-subtracted DRs, one has the following predictions for these subtraction constants, $\delta_3^{\rm pred} \simeq 1 m_\pi^{-4}$ and $\nu_3^{\rm pred} \simeq -2.5 m_\pi^{-6}$. An actual fit to the $^3D_1$ phase shifts only requires to vary $\nu_3^{(22)}$ around that value with the final result $\nu_3^{(22)} = -2.05(5)\, m_\pi^{-6}$, while $\delta_3^{(22)}$ stays put. Then only a relatively small change of around 20% in $\nu_3^{(22)}$ is necessary to end with a much better reproduction of the $^3D_1$ phase shifts that is compatible with PWA93, as shown by the hatched areas with (gray) parallel lines in Fig. 5(c) (denoted as NNLO-III results). Hence, this might be a natural NNNLO effect.

The fact that the matrix of limiting values $M_{ij} = \lim_{A\to-\infty} \Delta_{ij}(A)/(-A)^{3/2}$ has two negative eigenvalues is certainly related to the possibility of obtaining meaningful DRs with only one free parameter, according to the necessary condition of Ref. [44] to obtain meaningful once-subtracted DRs for $\lambda < 0$; cf. Sec. III B. Indeed, because the mixing between different partial waves is very small these eigenvalues are given in good approximation by M_{11} and M_{22}; this rule applies, in fact, not only to the $^3S_1$-$^3D_1$ coupled waves but to any other ones.

XI. COUPLED $^3P_2$-$^3F_2$ WAVES

This section is devoted to the study of the coupled wave system $^3P_2$-$^3F_2$. By direct computation one has in this case that

$$\lambda_{11} = \lim_{A\to-\infty} \frac{\Delta_{11}(A)}{(-A)^{3/2}} > 0, \tag{42}$$

which requires one to consider DRs with more than one subtraction for the $^3P_2$ wave [44]. Indeed, similarly to the $^3P_0$ and $^3P_1$ partial waves, discussed in Sec. V, one needs to take at least three subtractions in the DRs for the $^3P_2$ wave to obtain stable and meaningful results. The following three-times-subtracted DRs for the $^3P_2$ wave is used here:

$$\begin{aligned} D_{11}(A) &= 1 + \delta_2^{(11)} A + \delta_3^{(11)} A(A-C) \\ &\quad - \nu_2^{(11)} \frac{A(A-C)^2}{\pi} \int_0^\infty dq^2 \frac{\nu_{11}(q^2)}{(q^2-A)(q^2-C)^2} \\ &\quad - \nu_3^{(11)} \frac{A(A-C)^2}{\pi} \int_0^\infty dq^2 \frac{\nu_{11}(q^2) q^2}{(q^2-A)(q^2-C)^2} \\ &\quad + \frac{A(A-C)^2}{\pi} \int_{-\infty}^L dk^2 \frac{\Delta_{11}(k^2) D_{11}(k^2)}{(k^2)^3} \\ &\quad \times g_{11}(A, k^2, C; 2), \end{aligned} \tag{43}$$

$$N_{11}(A) = \nu_2^{(11)} A + \nu_3^{(11)} A^2 + \frac{A^3}{\pi} \int_{-\infty}^L dk^2 \frac{\Delta_{11}(k^2) D_{11}(k^2)}{(k^2)^3 (k^2 - A)}. \tag{44}$$

The standard formalism for the coupled waves, given in Eqs. (14) and (15), is employed with respect to the mixing and $^3F_2$ partial waves with $\ell_{12} = 2$ and $\ell_{22} = 3$, in order. As a result, two and three subtractions are taken, respectively.

As usual for the P waves, $\nu_2^{(11)} = 4\pi a_V/m$ by requiring the exact reproduction of the $^3P_2$ scattering volume extracted from PWA93 [47], $a_V = 0.0964 M_\pi^{-3}$, while $\nu_3^{(11)}$ is fitted to the results of this PWA. Regarding the subtraction constants $\delta_i^{(jj)}$, $i = 1$, 2, and 3, and $j = 1$ or 2, I follow the principle of maximal smoothness in virtue of which $\delta_2^{(jj)} = 0$ and fit $D_{jj}^{(1)}(-M_\pi^2)$.[18] The resulting fitted values are given in Table III, while the free

[18] In the following I use $D_{ij}^{(p-2)}(-M_\pi^2)$ as free parameter in terms of which one can calculate $\delta_p^{(ij)}$ from Eq. (16).

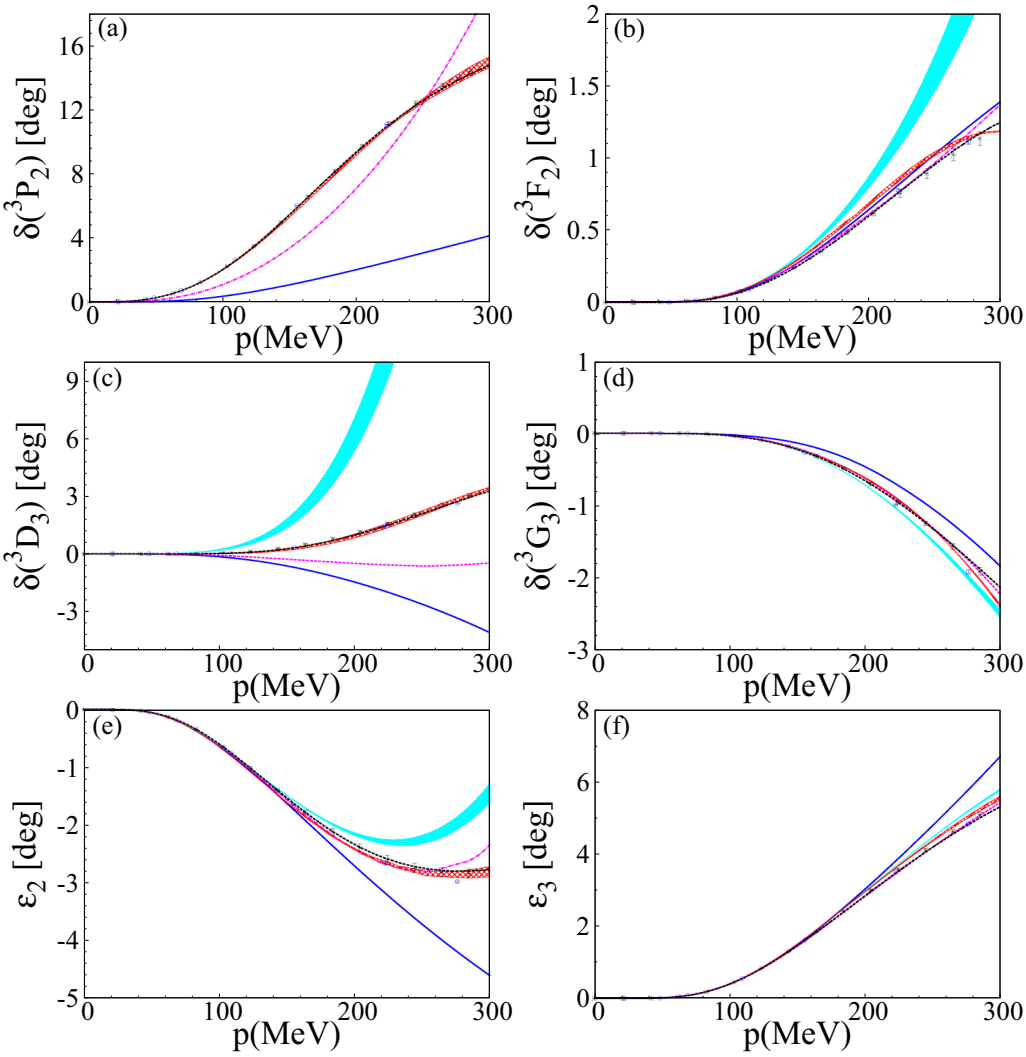

FIG. 6. Phase shifts for (a) ${}^3P_2$, (b) ${}^3F_2$, (c) ${}^3D_3$, (d) ${}^3G_3$, and the mixing angles (e) ε_2 and (f) ε_3. The (red) hatched areas correspond to the NNLO results and the (cyan) shaded ones to the perturbative phase shifts [46]. The meaning for the rest of the lines and points is the same as in Fig. 5.

parameter associated with the mixing wave is fixed to its pure perturbative value; cf. Sec. II C, $D_{12}(-M_\pi^2) = 1$. The resulting phase shifts are shown by the (red) hatched areas in Figs. 6(a) and 6(b) and the mixing angle ε_2 is shown in panel(e). There, one can see a clear improvement at NNLO in the reproduction of the ${}^3P_2$ phase shifts compared with the results at NLO, though this is achieved at the price of increasing the number of subtractions taken. The ${}^3F_2$ phase shifts and mixing angle ε_2 are reproduced with a quality similar to that already achieved at NLO.

The perturbative phase shifts in one-loop ChPT [46] are also shown by the (cyan) shaded bands in Fig. 6. I do not show them for the ${}^3P_2$ wave because a P wave cannot be considered peripheral. One sees that the full results provide a clear improvement in the reproduction of the PWA93 phase shifts and mixing angle with respect to the pure perturbative calculation. This improvement is obtained without dismissing the strength of the TPE at NNLO, as advocated in Ref. [50]. One should mention that the Born approximation phase shifts for ${}^3F_2$ and ${}^3F_3$ have a striking resemblance to the full NNLO results of Ref. [33] obtained within the Weinberg scheme. In addition, the (cyan) shaded bands in Fig. 6 for ε_2 and the ${}^3F_2$ phase shifts are also quite similar to those obtained in the dispersive study of Ref. [51]. This means that the full results are not so much sensitive to the particular set of c_i's taken as previously thought in the literature from the conclusions of Refs. [33,50].

XII. COUPLED ${}^3D_3$-${}^3G_3$ WAVES

For the study of the ${}^3D_3$-${}^3G_3$ coupled waves I follow the formalism for coupled waves, Eqs. (14) and (15), with $\ell_{11} = 2$, $\ell_{12} = 3$, and $\ell_{22} = 4$. Regarding the free parameters, the principle of maximal smoothness is invoked, although for the mixing wave the subtraction constants take their pure perturbative values. Hence, I fit to data $D_{11}(-M_\pi^2)$ and $D_{22}^{(2)}(-M_\pi^2)$; see Table III for the values obtained. The resulting phase shifts are shown by the (red) hatched areas in Figs. 6(c)

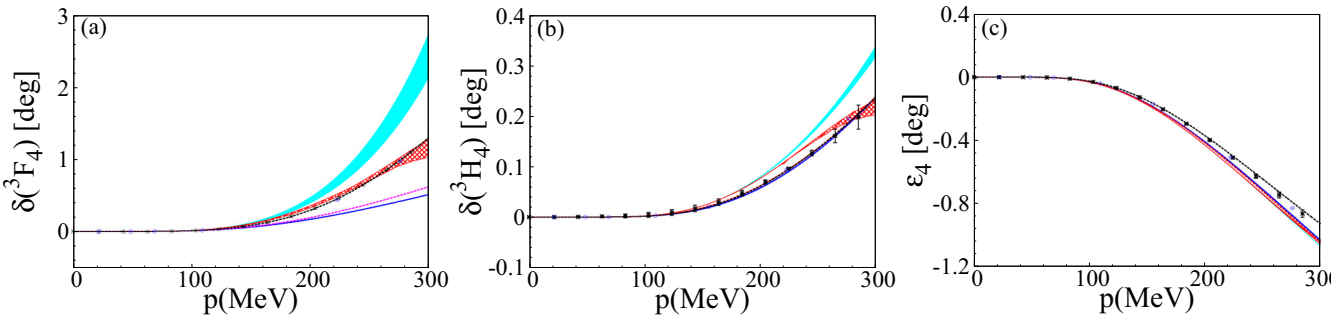

FIG. 7. Phase shifts for (a) $^3F_4$, (b) $^3H_4$, and the mixing angle (c) ε_4. The meanings of the lines are the same as in Fig. 6.

and 6(d), and the mixing angle ε_3 is shown in the last panel. An important point is that at NNLO the phase shifts for the $^3D_3$ wave follow closely the PWA93 phase shifts so that a remarkable improvement is obtained in comparison with both the NLO and perturbative results. Notice that this is accomplished without any need of dismissing the strength of TPE as directly obtained from the NLO πN amplitudes. The situation has been improved by taking into account the subtraction constant δ_2 or $D_{11}(-M_\pi^2)$, whose presence is required by the nonperturbative unitarity implementation[19] at NNLO; cf. Eq. (24). One also observes a good reproduction of the PWA93 results for the waves $^3G_3$ and ε_3, which are already well reproduced at NLO [44], as shown by the (magenta) dot-dashed lines.

XIII. COUPLED $^3F_4$-$^3H_4$ WAVES

The discussion of the $^3F_4$-$^3H_4$ coupled-wave system follows the standard formalism for coupled waves, Eqs. (14) and (15), with $\ell_{11} = 3$, $\ell_{12} = 4$, and $\ell_{22} = 5$. The free parameters are then fitted to data according to the principle of maximal smoothness, though for $^3H_4$ and the mixing partial wave, the subtraction constants are fixed to their pure perturbative values. Then one only needs to fit at the end $D_{11}^{(1)}(-M_\pi^2)$ to the PWA93 results, which value is given in Table III. The phase shifts and mixing angle obtained are shown by the (red) hatched areas in Fig. 7, and the width of each band reflects the dependence on the values of the πN NLO counterterms.

One can observe a clear improvement in the description of the $^3F_4$ phase shifts compared with the results from OPE (blue dotted lines), NLO (magenta dot-dashed lines), and perturbative approximation (cyan shaded areas). Analogously to the $^3D_3$ wave in the previous section, this improvement is related to the effect of the subtraction constant $\delta_3^{(11)}$ without any need to modify $\Delta(A)$ as calculated at NNLO in ChPT. Let us recall that the subtraction constants $\delta_p^{(ij)}$ arise because of the rescattering process that the N/D method allows to treat in a clear and well-defined way, overcoming the obscurities that still remain in the literature associated with the use of the cutoff regularized Lippmann-Schwinger with a higher-order *NN* potential. For the mixing angle ε_4 the quality in the reproduction of data is similar to that obtained by the other approximations just quoted. However, for the $^3H_4$ phase shifts the outcome at NNLO is a bit worse than at NLO and OPE, though one should also notice the tiny values for the $^3H_4$ phase shifts so that this discrepancy is certainly small in absolute value. It also cannot be removed by releasing the other subtraction constants $\delta_p^{(22)}$, with $p = 2$, 3, and 4. Likely, the origin of this difference in the $^3H_4$ phase shifts between the full results and PWA93 can be tracked back to the change in the leading Born approximation once the $\mathcal{O}(p^3)$ two-nucleon irreducible contributions are included in $\Delta_{22}(A)$.

XIV. CONCLUSIONS

I have discussed in this paper the application of the N/D method when its dynamical input, namely, the imaginary part of the *NN* partial waves along the LHC, is calculated in ChPT up to NNLO. It then comprises OPE, leading and subleading two-nucleon irreducible TPE, and once-iterated OPE [46]. A quite good reproduction of the Nijmegen PWA phase shifts and mixing angles has been obtained, in better agreement than the one achieved in the previous lower-order studies at LO [42,43] and NLO [44]. In particular, the NNLO results, without increasing the number of subtractions, provide clearly improved phase shifts for the partial waves $^1P_1$, $^1D_2$, $^3D_2$, $^3F_3$, $^3S_1$, ε_1, ε_2, $^3D_3$, and $^3F_4$ compared to the NLO case. This indicates that increasing the accuracy in the calculation of $\Delta(A)$ by performing the ChPT calculation at $\mathcal{O}(p^3)$ has a neat impact in increasing the quality of the results, clearly indicating the importance of chiral symmetry in *NN* dynamics. Especially notorious is the systematic improvement for the triplet partial waves with with $\ell_{11} = J - 1$, $^3P_2$, $^3D_3$, and $^3F_4$, such that now the associated phase shifts are accurately reproduced while at NLO they were not properly accounted for. To obtain such a good agreement with the Nijmegen PWA, one does not need to fine-tune the low-energy pion-nucleon constants c_i, contrarily to common wisdom, but just take directly their values from pion-nucleon scattering. The point that stems from this study is that one should perform in a well-defined way the iteration of diagrams along the RHC, which are responsible for unitarity and analyticity attached to this cut, rather than reshuffling the *NN* potential with contributions from higher orders. In this respect, the use of DRs allows one to perform the iteration of two-nucleon intermediate states independently of regulator.

[19] In more general terms, this is done by keeping the right analytical properties of *NN* partial waves while respecting unitarity in the full amplitudes.

I have also compared the full results for the higher partial waves with the perturbative phase shifts from the one-loop ChPT calculation of Ref. [46], which typically is much more dependent on the values of the c_i's than the final results. From this comparison, as well as from the direct study of the importance of the different contributions of $\Delta(A)$ to the dispersive integrals, it follows that the *NN D* waves cannot be treated perturbatively.

It is worth noting that a chiral power counting for the subtraction constants has been established, so that twice-subtracted DRs are appropriate when $\Delta(A)$ is calculated at NLO and NNLO. From these considerations it turns out that the chiral power expansion is made over a scale $\Lambda \approx 400$ MeV. Let us notice that a close reproduction of data for all the partial waves is obtained once the criteria exposed at the end of Sec. III B are fulfilled, that is, either (i) having two subtractions at NNLO according to the chiral power counting for the subtraction constants [Eq. (24)], (ii) having $\ell \geqslant 3$ subtractions ($J \geqslant 3$ for the mixing partial waves) to satisfy the right threshold behavior for the higher partial waves, or (iii) introducing as many subtractions as needed to end with a meaningful IE. Owing to this last requirement, three-times-subtracted DRs are needed for the *P* waves, because for them $\lambda > 0$ [Eqs. (30) and (42)], except for the $^1P_1$ wave, for which twice-subtracted DRs are enough. This could be a specific feature for the NNLO calculation of $\Delta(A)$ for the *P* waves that has to be investigated at higher orders.[20] The only case where one more subtraction is included without being necessary according to the points (i)–(iii) above is for the wave $^3D_1$. This is studied at the end of Sec. X to show that the remaining disagreement with data at NNLO might be considered naturally a NNNLO effect. Twice-subtracted DRs, according to (i), have been finally used for the waves $^1S_0$, $^1P_1$, $^1D_2$, $^2D_2$, $^3S_1$-$^3D_1$, ϵ_2, and $^3D_3$.

Last but not least, up to the order studied here one confirms the long-range correlation between the effective ranges and the scattering lengths for the *NN S* waves when only once-subtracted DRs are applied. In this way one can predict values for the *S*-wave effective ranges in agreement with experiment up to around a 10%. For future prospects, one should consider the impact of higher in $\Delta(A)$, which are partially calculated already in the literature, as an interesting extension of the present work to settle the applicability of the approach based on the N/D method to *NN* scattering in ChPT with a high degree of accurateness. Another issue that requires more study is to establish the relationship between the subtraction constants and the counterterms present in the *NN* chiral Lagrangians.

ACKNOWLEDGMENTS

I would like to thank Álvaro Calle Cordón, Enrique Ruiz Arriola, and David Rodríguez Entem for interesting discussions and the latter also for a critical reading of the manuscript. I acknowledge Enrique Ruiz Arriola and Rodrigo Navarro Pérez for sending me the AV18 phase shifts. This work is partially funded by the grants from MINECO (Spain) and ERDF (EU), Grants No. FPA2010-17806 and No. FPA2014-40483-P, and from the Fundación Séneca, Grant No. 11871/PI/09. I am also thankful for partial financial support from the EU-Research Infrastructure Integrating Activity "Study of Strongly Interacting Matter" (HadronPhysics2, Grant No. 227431) under the Seventh Framework Program of EU, the Consolider-Ingenio 2010 Programme CPAN (Grant No. CSD2007-00042), and the Spanish Excellence Network on Hadronic Physics Grant No. FIS2014-57026-REDT.

APPENDIX: CALCULATION OF HIGHER-ORDER SHAPE PARAMETERS

Let us explain first the method for the $^1S_0$ partial wave, which is then straightforwardly generalized to the $^3S_1$ case. Taking into account elastic unitarity, one has that

$$H(A) \equiv \frac{4\pi}{mT(A)} + i\sqrt{A} = \sqrt{A}\cot\delta \tag{A1}$$

is an analytical function of A that has no (elastic) unitarity cut because it obeys the Schwarz reflection principle and it is real for $A > 0$. Then it admits a Taylor expansion around $A = 0$ with a radius of convergence equal to $M_\pi^2/4$ because its first singularity is attributable to the onset of the LHC at $A = -M_\pi^2/4$. This expansion is the so-called ERE. One can calculate the function $H(A)$ for complex A in a direct way from the DRs employed above to calculate $T(A) = N(A)/D(A)$. Nonetheless, care has to be taken when employing $g(A,k^2)$ from Eq. (7) because one should guarantee that $\sqrt{A}$ is defined in the first Riemann sheet; that is, $\mathrm{Im}\sqrt{A} > 0$ must be enforced for all $A \in \mathbb{C}$. The same requirement should be also fulfilled by the $\sqrt{A}$ that appears explicitly in the definition of $H(A)$.

The nth-order derivative of $H(A)$ at $A = 0$ can be calculated by making use of the Cauchy integral formula

$$H^{(n)}(0) = \frac{n!}{2\pi i}\oint_\gamma dz \frac{H(z)}{z^{n+1}}, \tag{A2}$$

where γ is a close contour inside the ball of radius $M_\pi^2/4$ and taken counterclockwise. In practical terms the contour γ is taken as a circle of radius $R < M_\pi^2/4$ with $z = R\exp i\phi$ and $\phi \in [0,2\pi]$. A good numerical check of the procedure is the stability of the derivative calculated from the previous equation independently of the value taken for $0 < R < M_\pi^2/4$. Thus, one obtains

$$a_s^{-1} = -\frac{1}{2i\pi}\oint dz\frac{H(z)}{z}, \quad r_s = \frac{1}{i\pi}\oint dz\frac{H(z)}{z^2},$$
$$v_i = \frac{1}{2i\pi}\oint dz\frac{H(z)}{z^{i+1}}. \tag{A3}$$

One can proceed in the same way for the $^3S_1$-$^3D_1$ coupled wave system in terms of the eigenvalue S_0 given by

$$S_0 = \frac{1}{2}\left[S_{11} + S_{22} + (S_{11} - S_{22})\sqrt{1 + \left(\frac{2S_{12}}{S_{11} - S_{22}}\right)^2}\right]. \tag{A4}$$

[20] Were $\lambda < 0$, one would have invoked less free parameters for the *P* waves than in Table III.

Then one defines in terms of it the corresponding uncoupled partial wave,

$$T_0(A) = \frac{S_0 - 1}{2i\rho(A)}, \tag{A5}$$

where the definition of $\rho(A)$ in Eq. (3) should be taken in the first Riemann sheet. An analogous function to $H(A)$ in Eq. (A1) is then constructed from $T_0(A)$ and one can calculate the different parameters in the ERE of Eq. (39) as in Eq. (A3).

[1] S. Weinberg, Phys. A (Amsterdam, Neth.) **96**, 327 (1979).
[2] J. Gasser and H. Leutwyler, Ann. Phys. **158**, 142 (1984); Nucl. Phys. B **250**, 465 (1985).
[3] J. A. Oller and E. Oset, Nucl. Phys. A **620**, 438(E) (1997); **652**, 407 (1999).
[4] J. A. Oller and E. Oset, Phys. Rev. D **60**, 074023 (1999).
[5] J. A. Oller and L. Roca, Phys. Lett. B **651**, 139 (2007).
[6] J. A. Oller, L. Roca, and C. Schat, Phys. Lett. B **659**, 201 (2008).
[7] M. Albaladejo and J. A. Oller, Phys. Rev. D **86**, 034003 (2012).
[8] B. Ananthanarayan, G. Colangelo, J. Gasser, and H. Leutwyler, Phys. Rep. **353**, 207 (2001).
[9] T. N. Truong, Phys. Rev. Lett. **61**, 2526 (1988).
[10] J. Gasser, H. Leutwyler, and M. E. Sainio, Phys. Lett. B **253**, 252 (1991); **253**, 260 (1991).
[11] J. M. Alarcon, J. M. Camalich, and J. A. Oller, Ann. Phys. **336**, 413 (2013).
[12] J. M. Alarcon, J. M. Camalich, and J. A. Oller, Phys. Rev. D **85**, 051503 (2012).
[13] J. Gasser, M. E. Sainio, and A. Svarc, Nucl. Phys. B **307**, 779 (1988).
[14] E. E. Jenkins and A. V. Manohar, Phys. Lett. B **255**, 558 (1991).
[15] J. M. Alarcon, L. S. Geng, J. M. Camalich, and J. A. Oller, Phys. Lett. B **730**, 342 (2014).
[16] J. Gegelia and G. Japaridze, Phys. Rev. D **60**, 114038 (1999); T. Fuchs, J. Gegelia, G. Japaridze, and S. Scherer, *ibid.* **68**, 056005 (2003).
[17] V. Pascalutsa, M. Vanderhaegen, and S. N. Yang, Phys. Rep. **437**, 125 (2007); V. Pascalutsa and D. R. Phillips, Phys. Rev. C **67**, 055202 (2003).
[18] J. Bijnens, PoS CD **09**, 031 (2009); Prog. Part. Nucl. Phys. **58**, 521 (2007).
[19] G. Ecker, Nucl. Phys. Proc. Suppl. **245**, 1 (2013); Prog. Part. Nucl. Phys. **35**, 1 (1995).
[20] V. Bernard, Prog. Part. Nucl. Phys. **60**, 82 (2008).
[21] A. Pich, Rep. Prog. Phys. **58**, 563 (1995); in *Proceedings of the Les Houches Summer School of Theoretical Physics*, edited by F. David and R. Gupta (Elsevier Science, Amsterdam, 1999), Vol. II.
[22] U.-G. Meißner, Rep. Prog. Phys. **56**, 903 (1993).
[23] V. Bernard, N. Kaiser, and U.-G. Meißner, Int. J. Mod. Phys. E **04**, 193 (1995).
[24] S. Weinberg, Phys. Lett. B **251**, 288 (1990); Nucl. Phys. B **363**, 3 (1991).
[25] J. A. Oller, A. Lacour, and U.-G. Meißner, J. Phys. G **37**, 015106 (2010); A. Lacour, J. A. Oller, and U.-G. Meißner, Ann. Phys. **326**, 241 (2011).
[26] E. Epelbaum, H.-W. Hammer, and U.-G. Meißner, Rev. Mod. Phys. **81**, 1773 (2009).
[27] R. Machleidt and D. R. Entem, Phys. Rep. **503**, 1 (2011).
[28] E. Epelbaum, Prog. Part. Nucl. Phys. **57**, 654 (2006).
[29] P. F. Bedaque and U. van Kolck, Annu. Rev. Nucl. Part. Sci. **52**, 339 (2002).
[30] U. van Kolck, Prog. Part. Nucl. Phys. **43**, 337 (1999).
[31] C. Ordóñez, L. Ray, and U. van Kolck, Phys. Lett. B **291**, 459 (1992); Phys. Rev. Lett. **72**, 1982 (1994); Phys. Rev. C **53**, 2086 (1996).
[32] D. R. Entem and R. Machleidt, Phys. Lett. B **524**, 93 (2002); Phys. Rev. C **66**, 014002 (2002); **68**, 041001 (2003).
[33] E. Epelbaum, Ph.D. thesis, published in Berichte des Forschungszentrum Jülich, No. 3803, Jülich, 2000; E. Epelbaum, W. Gloeckle, and U.-G. Meißner, Nucl. Phys. A **671**, 295 (2000).
[34] E. Epelbaum, W. Gloeckle, and U.-G. Meißner, Nucl. Phys. A **747**, 362 (2005).
[35] M. Pavón Valderrama and E. Ruiz Arriola, Phys. Rev. C **74**, 054001 (2006); **74**, 064004 (2006); **72**, 054002 (2005).
[36] A. Nogga, R. G. E. Timmermans, and U. van Kolck, Phys. Rev. C **72**, 054006 (2005).
[37] D. B. Kaplan and M. J. Savage, Phys. Lett. B **365**, 244 (1996); D. B. Kaplan, M. J. Savage, and M. B. Wise, Nucl. Phys. B **478**, 629 (1996).
[38] C.-J. Yang, C. Elster, and D. R. Phillips, Phys. Rev. C **77**, 014002 (2008); **80**, 034002 (2009); **80**, 044002 (2009).
[39] M. Pavon Valderrama, Phys. Rev. C **84**, 064002 (2011).
[40] B. Long and C. J. Yang, Phys. Rev. C **84**, 057001 (2011); **85**, 034002 (2012); **86**, 024001 (2012).
[41] C. Zeoli, R. Machleidt, and D. R. Entem, Few Body Syst. **54**, 2191 (2013).
[42] M. Albaladejo and J. A. Oller, Phys. Rev. C **84**, 054009 (2011).
[43] M. Albaladejo and J. A. Oller, Phys. Rev. C **86**, 034005 (2012).
[44] Z.-H. Guo, J. A. Oller, and G. Ríos, Phys. Rev. C **89**, 014002 (2014).
[45] G. F. Chew and S. Mandelstam, Phys. Rev. **119**, 467 (1960).
[46] N. Kaiser, R. Brockmann, and W. Weise, Nucl. Phys. A **625**, 758 (1997).
[47] V. G. J. Stoks, R. A. M. Klomp, M. C. M. Rentmeester, and J. J. de Swart, Phys. Rev. C **48**, 792 (1993).
[48] M. Pavon Valderrama and E. Ruiz Arriola, Ann. Phys. **323**, 1037 (2008).
[49] D. R. Entem, E. Ruiz Arriola, M. Pavon Valderrama and R. Machleidt, Phys. Rev. C **77**, 044006 (2008).
[50] E. Epelbaum, W. Gloeckle, and U.-G. Meißner, Eur. Phys. J. A **19**, 125 (2004); **19**, 401 (2004).
[51] A. M. Gasparyan, M. F. M. Lutz, and E. Epelbaum, Eur. Phys. J. A **49**, 115 (2013).
[52] A. Gasparyan and M. F. M. Lutz, Nucl. Phys. A **848**, 126 (2010).
[53] A. M. Gasparyan and M. F. M. Lutz, Fizika B **20**, 55 (2011).
[54] A. M. Gasparyan, M. F. M. Lutz, and B. Pasquini, Nucl. Phys. A **866**, 79 (2011).
[55] I. V. Danilkin, L. I. R. Gil, and M. F. M. Lutz, Phys. Lett. B **703**, 504 (2011).
[56] I. V. Danilkin, M. F. M. Lutz, S. Leupold, and C. Terschlusen, Eur. Phys. J. C **73**, 2358 (2013).

[57] S. Fleming, T. Mehen, and I. W. Stewart, Phys. Rev. C **61**, 044005 (2000); Nucl. Phys. A **677**, 313 (2000).
[58] V. G. J. Stoks, R. A. M. Klomp, C. P. F. Terheggen, and J. J. de Swart, Phys. Rev. C **49**, 2950 (1994).
[59] R. B. Wiringa, V. G. J. Stoks, and R. Schiavilla, Phys. Rev. C **51**, 38 (1995); S. Veerasamy and W. N. Polyzou, *ibid.* **84**, 034003 (2011).
[60] R. Navarro Pérez, J. E. Amaro, and E. Ruiz Arriola, Phys. Rev. C **88**, 024002 (2013); **88**, 069902 (2013).
[61] A. D. Martin and T. D. Spearman, *Elementary Particle Theory* (North-Holland, Amsterdam, 1970).
[62] L. Castillejo, R. H. Dalitz, and F. J. Dyson, Phys. Rev. **101**, 453 (1956).
[63] H. P. Stapp, T. J. Ypsilantis, and N. Metropolis, Phys. Rev. **105**, 302 (1957).
[64] M. Lutz, Nucl. Phys. A **677**, 241 (2000).
[65] R. Higa and M. R. Robilotta, Phys. Rev. C **68**, 024004 (2003); M. R. Robilotta, *ibid.* **63**, 044004 (2001).
[66] E. Epelbaum and J. Gegelia, Phys. Lett. B **716**, 338 (2012).
[67] R. Koch, Nucl. Phys. A **448**, 707 (1986).
[68] R. A. Arndt, W. J. Briscoe, I. I. Strakovsky, and R. L. Workman, Phys. Rev. C **74**, 045205 (2006), and references therein; computer code SAID, online program at http://gwdac.phys.gwu.edu/.
[69] H. Krebs, A. Gasparyan, and E. Epelbaum, Phys. Rev. C **85**, 054006 (2012).
[70] J. M. Alarcon, J. M. Camalich, J. A. Oller, and L. Alvarez-Ruso, Phys. Rev. C **83**, 055205 (2011).
[71] M. C. M. Rentmeester, R. G. E. Timmermans, and J. J. de Swart, Phys. Rev. C **67**, 044001 (2003).
[72] P. Buettiker and U.-G. Meißner, Nucl. Phys. A **668**, 97 (2000).
[73] N. Fettes and U.-G. Meißner, Nucl. Phys. A **676**, 311 (2000); N. Fettes, U.-G. Meißner, and S. Steininger, *ibid.* **640**, 199 (1998).
[74] M. Birse, Philos. Trans. R. Soc., A **369**, 2662 (2011).
[75] E. Epelbaum and J. Gegelia, Eur. Phys. J. A **41**, 341 (2009).
[76] V. V. Flambaum, G. F. Gribakin, and C. Harabati, Phys. Rev. A **59**, 1998 (1999); G. F. Gribakin and V. V. Flambaum, *ibid.* **48**, 546 (1993).
[77] A. Calle Cordon and E. Ruiz Arriola, Phys. Rev. A **81**, 044701 (2010).
[78] V. Bernard, N. Kaiser, and U.-G. Meißner, Phys. Lett. B **309**, 421 (1993).
[79] E. Epelbaum, H. Krebs, and U.-G. Meißner, Eur. Phys. J. A **51**, 53 (2015).
[80] M. M. Nagels, T. A. Rijken, and J. J. de Swart, Phys. Rev. D **17**, 768 (1978).
[81] J. J. de Swart, C. P. F. Terheggen, and V. G. J. Stoks, *Proceedings of 3rd International Symposium on Dubna Deuteron 95*, Dubna, Moscow, July 4–7, 1995, arXiv:nucl-th/9509032.
[82] T. D. Cohen and J. M. Hansen, Phys. Rev. C **59**, 13 (1999).
[83] N. L. Rodning and L. D. Knutson, Phys. Rev. C **41**, 898 (1990).
[84] T. E. O. Ericson and M. Rosa-Clot, Phys. Lett. B **110**, 193 (1982); Nucl. Phys. A **405**, 497 (1983).
[85] H. E. Conzett, F. Hinterberger, P. von Rossen, F. Seiler, and E. J. Stephenson, Phys. Rev. Lett. **43**, 572 (1979).
[86] S. Klarsfeld, J. Martorell, and D. W. L. Sprung, J. Phys. G: Nucl. Phys. **10**, 165 (1984).
[87] M. Pavon Valderrama and E. Ruiz Arriola, Phys. Rev. C **83**, 044002 (2011).